



Article

Distribution and Chemistry of Phoenixin-14, a Newly Discovered Sensory Transmission Molecule in Porcine Afferent Neurons

Urszula Mazur ^{1,*}, Ewa Lepiarczyk ¹, Paweł Janikiewicz ¹, Elżbieta Łopieńska-Biernat ²,
Mariusz Krzysztof Majewski ¹ and Agnieszka Bossowska ¹

- ¹ Department of Human Physiology and Pathophysiology, University of Warmia and Mazury in Olsztyn, Warszawska 30, 10-082 Olsztyn, Poland; ewa.lepiarczyk@uwm.edu.pl (E.L.); pawel.janikiewicz@uwm.edu.pl (P.J.); mariusz.majewski@uwm.edu.pl (M.K.M.); agnieszka.bossowska@uwm.edu.pl (A.B.)
- ² Department of Biochemistry, Faculty of Biology and Biotechnology, University of Warmia and Mazury in Olsztyn, Oczapowskiego 1A, 10-719 Olsztyn, Poland; ela.lopienska@uwm.edu.pl
- * Correspondence: urszula.mazur@uwm.edu.pl; Tel.: +48-89-524-56-42

Abstract: Phoenixin-14 (PNX), initially discovered in the rat hypothalamus, was also detected in dorsal root ganglion (DRG) cells, where its involvement in the regulation of pain and/or itch sensation was suggested. However, there is a lack of data not only on its distribution in DRGs along individual segments of the spinal cord, but also on the pattern(s) of its co-occurrence with other sensory neurotransmitters. To fill the above-mentioned gap and expand our knowledge about the occurrence of PNX in mammalian species other than rodents, this study examined (i) the pattern(s) of PNX occurrence in DRG neurons of subsequent neuromeres along the porcine spinal cord, (ii) their intraganglionic distribution and (iii) the pattern(s) of PNX co-occurrence with other biologically active agents. PNX was found in approximately 20% of all nerve cells of each DRG examined; the largest subpopulation of PNX-positive (PNX⁺) cells were small-diameter neurons, accounting for 74% of all PNX-positive neurons found. PNX⁺ neurons also co-contained calcitonin gene-related peptide (CGRP; 96.1%), substance P (SP; 88.5%), nitric oxide synthase (nNOS; 52.1%), galanin (GAL; 20.7%), calcitonin (CRT; 10%), pituitary adenylate cyclase-activating polypeptide (PACAP; 7.4%), cocaine and amphetamine related transcript (CART; 5.1%) or somatostatin (SOM; 4.7%). Although the exact function of PNX in DRGs is not yet known, the high degree of co-localization of this peptide with the main nociceptive transmitters SP and CGRP may suggest its function in modulation of pain transmission.

Keywords: phoenixin-14 (PNX); pig; dorsal root ganglia (DRG); neuropeptides; immunofluorescence; mass spectrometry



Citation: Mazur, U.; Lepiarczyk, E.; Janikiewicz, P.; Łopieńska-Biernat, E.; Majewski, M.K.; Bossowska, A. Distribution and Chemistry of Phoenixin-14, a Newly Discovered Sensory Transmission Molecule in Porcine Afferent Neurons. *Int. J. Mol. Sci.* **2023**, *24*, 16647. <https://doi.org/10.3390/ijms242316647>

Academic Editor: Ivana Caputo

Received: 24 October 2023

Revised: 18 November 2023

Accepted: 21 November 2023

Published: 23 November 2023



Copyright: © 2023 by the authors. Licensee MDPI, Basel, Switzerland. This article is an open access article distributed under the terms and conditions of the Creative Commons Attribution (CC BY) license (<https://creativecommons.org/licenses/by/4.0/>).

1. Introduction

Phoenixin-14 (PNX), first described by Yosten et al. in 2013 [1], was initially linked to reproductive system control, due to the high expression of this peptide in the rodent hypothalamus and pituitary gland, where, by acting through the orphan receptor G protein-coupled receptor 173 (GPR173), PNX was found to activate gonadotropin-releasing hormone-secreting cells, leading to the release of luteinizing hormone or follicle-stimulating hormone by pituitary gonadotrophs [1,2]. Nine years after PNX's identification, further studies revealed that the presence of this peptide is not limited to the hypothalamo-pituitary complex and an engagement of PNX in the central control of several other biological processes, including food intake, energy homeostasis, water balance and modulation of inflammation or memory and anxiety, has also been reviewed [3,4].

2.2. Distribution Pattern and Morphometrical Characteristics of PN_X-Containing Sensory Neurons in Studied DRGs

2.2.1. Distribution Pattern of PN_X⁺ Neurons

PN_X⁺ nerve cells were observed bilaterally in all the studied DRGs. The total number of PN_X⁺ sensory neurons counted in all the studied DRGs per animal ranged from 16714 to 19675 (18481 ± 1562 ; mean \pm standard deviation—SD), representing $19.7 \pm 1.0\%$ of all the sensory neurons counted in the investigated DRG. In the left ganglia, the number of PN_X-containing sensory neurons ranged from 7806 to 9963 per animal (9092 ± 1137) and accounted for $19.1 \pm 0.6\%$ of all the sensory neurons. Very similar results regarding both the number and percentage of PN_X⁺ nerve cells were obtained in the right ganglia in which the number of PN_X-labeled perikarya ranged from 8908 to 9712 per animal (9390 ± 425) and accounted for $19.3 \pm 1.5\%$ of all the sensory neurons.

The PN_X⁺ sensory neurons were observed in all the selected C, Th, L and S DRG ($20.2 \pm 1.4\%$, $16.5 \pm 1.5\%$, $19.4 \pm 1.0\%$ and $21.4 \pm 2.5\%$, respectively). No statistically significant differences in the number of PN_X-containing sensory nerve cells were observed between the left and right ganglia from the same level of the spinal cord and between the ganglia located in various levels of the spinal cord examined. Details concerning the relative frequency of PN_X⁺ sensory neurons observed in the selected left and the right DRG taken from the C, Th, L and S levels of the spinal cord are shown in Table 1 and Figure 2.

Table 1. Relative frequency of PN_X-positive (PN_X⁺) neuronal profiles located in the left and right DRGs of the cervical (C), thoracic (Th), lumbar (L) and sacral (S) levels of the spinal cord. The obtained data were pooled for each animal and are presented as mean \pm standard deviation (SD) (N = 6 animals).

DRG	Segments of the Spinal Cord (%)										
	C1	C4	C7	Th1	Th7	Th15	L1	L3	L6	S1	S3
left	21.5 \pm 3.9	17.5 \pm 3.1	21.9 \pm 1.7	16.2 \pm 2.0	17.3 \pm 0.7	15.4 \pm 2.3	17.8 \pm 2.4	16.3 \pm 0.8	23.3 \pm 3.6	22.8 \pm 2.0	20.4 \pm 4.6
right	18.5 \pm 7.2	21.1 \pm 6.6	20.9 \pm 1.0	16.8 \pm 1.9	17.2 \pm 0.6	16.1 \pm 3.7	15.7 \pm 4.1	17.6 \pm 2.0	25.8 \pm 1.2	24.6 \pm 0.9	18.0 \pm 7.6

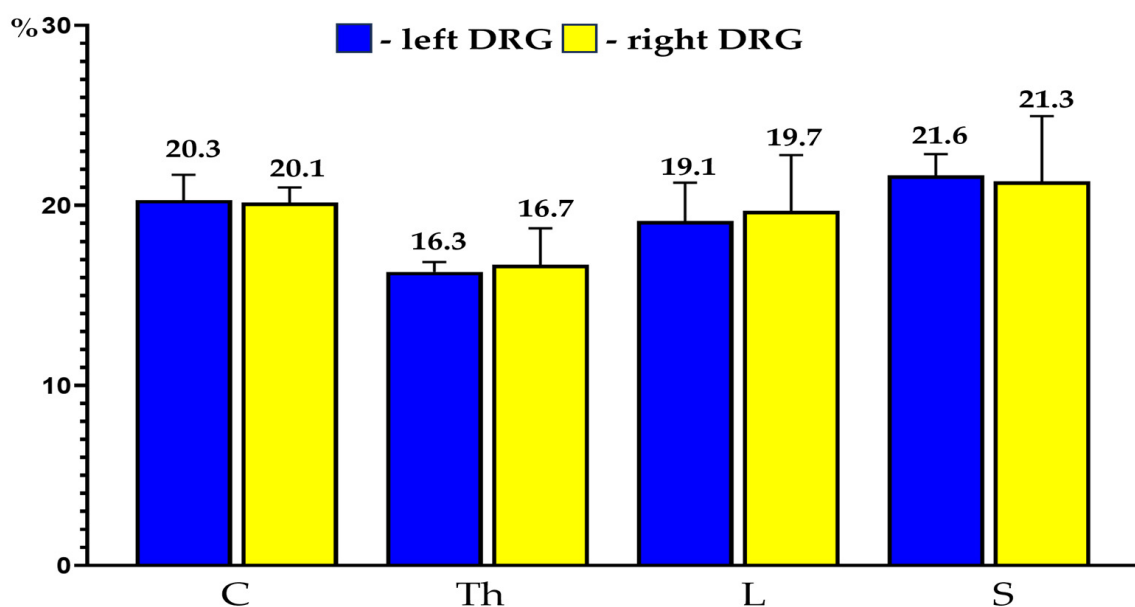


Figure 2. Bar diagram showing the relative percentages of PN_X⁺ sensory neurons located in the left (blue bars) and the right (yellow bars) DRGs of the C, Th, L and S segments of the spinal cord. The obtained data were pooled for each animal and are presented as mean \pm SD (N = 6 animals).

2.2.2. Morphometrical Characteristics of PN^X⁺ Neurons

In the present study, the PN^X⁺ DRG neurons belonged to all cell sizes: small (SI) (neurons with an average diameter of up to 40 μm), medium (M) (neurons with a diameter from 41 μm to 70 μm) and large (Lg) (neurons with a diameter up to 71 μm). In general, the vast majority of PN^X⁺ sensory neurons belonged to SI-sized cells (73.9 ± 4.7%) which prevailed over the M-sized sensory neurons (24.9 ± 4.7%), while the Lg nerve cells (1.2 ± 0.8%) were only occasionally found in all the DRGs studied. There were no significant differences in the number of PN^X-containing sensory neurons belonging to these three size classes between the left and the right DRGs. When comparing the relative frequencies of SI, M and Lg perikarya in the left and right DRGs, SI cells constituted the largest population of PN^X⁺ neurons (70.6 ± 13.9% vs. 73.8 ± 4.9%) and M-sized cells constituted a smaller population (24.8 ± 5.3% vs. 25.1 ± 4.9%), while only a few Lg-sized cells (1.0 ± 0.9% vs. 1.1 ± 0.8%) were found. Moreover, no statistically significant differences in the number of PN^X-labeled neurons belonging to the SI-, M- and Lg-sized populations of sensory nerve cells were observed between the C, Th, L and S DRGs. The details on the relative frequency of PN^X⁺ sensory neurons of the different size classes in the selected left and the right DRGs at the C, Th, L and S levels of the spinal cord are shown in Table 2 and Figure 3. Representative images of the PN^X⁺ DRG nerve cells belonging to the different size classes are shown in Figure 4.

Table 2. Percentages of PN^X⁺ neuronal populations of different sizes (small—SI; medium—M; large—Lg) located in the left and the right DRGs of the C, Th, L and S segments of the spinal cord. The obtained data were pooled for each animal and are presented as mean ± SD (N = 6 animals).

DRG	Segments of The Spinal Cord (%)											
	C			Th			L			S		
	SI	M	Lg	SI	M	Lg	SI	M	Lg	SI	M	Lg
left	74.7 ± 3.1	23.9 ± 2.3	1.4 ± 0.9	70.6 ± 3.1	28.5 ± 2.9	0.9 ± 0.3	75.4 ± 5.9	23.8 ± 5.8	0.8 ± 0.6	76.3 ± 1.0	21.9 ± 0.8	1.8 ± 0.2
right	76.7 ± 3.1	22.1 ± 2.9	1.2 ± 0.6	71.4 ± 4.9	27.8 ± 4.7	0.8 ± 0.7	72.4 ± 5.2	26.6 ± 5.2	1.0 ± 0.6	75.4 ± 4.8	22.5 ± 4.8	2.1 ± 0.9

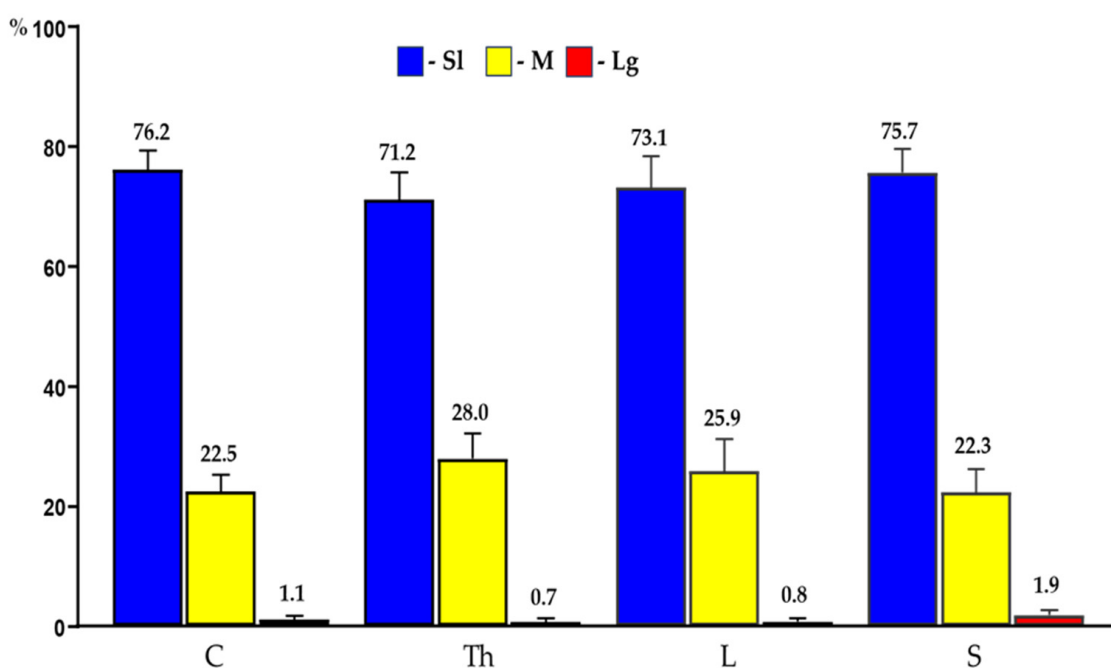


Figure 3. Bar diagram summarizing the percentages of differently sized (SI; M; Lg) PN^X⁺ sensory nerve cells found in C, Th, L and S segments of the spinal cord. The obtained data were pooled for each animal and are presented as mean ± SD (N = 6 animals).

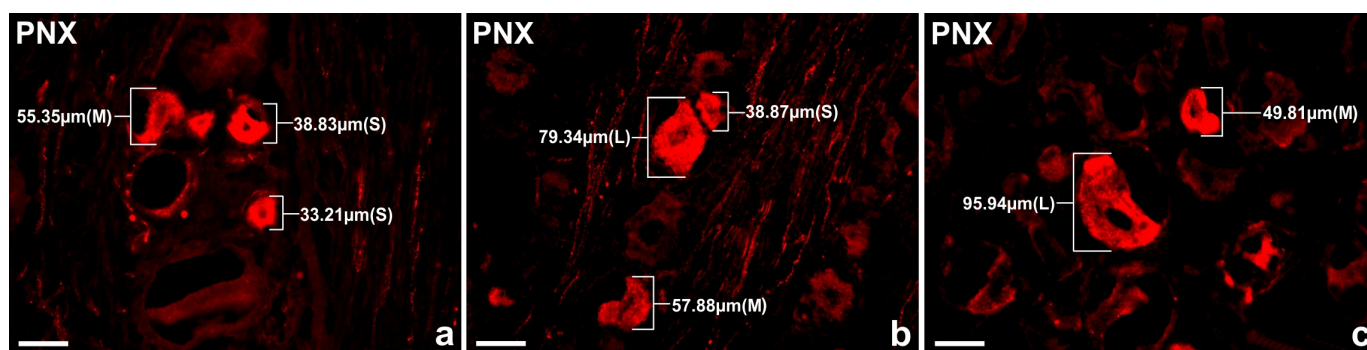


Figure 4. Representative images of the PNx⁺ nerve cells in the porcine DRG L1 belonging to the different size classes: (a) SI cells (33.21 μm, 38.83 μm), M cells (55.35 μm); (b) SI cell (38.87 μm), M cell (57.88 μm), Lg cell (79.34 μm); (c) M cell (49.81 μm), Lg cell (95.94 μm). Scale bar: 50 μm.

2.2.3. Intraganglionic Distribution Patterns of PNx⁺ Neurons

To determine the intraganglionic distribution pattern(s) of the PNx⁺ sensory neurons in all the studied DRGs, the ‘mask’ shown in Figure 5 was applied to each analyzed ganglion section.

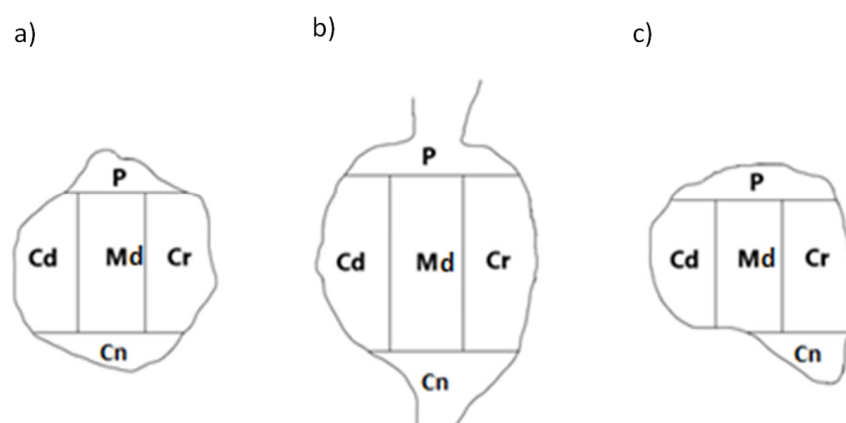


Figure 5. A schematic diagram of the DRG section showing its arbitrary division into topographical domains and in which, the occurrence and relative frequency of PNx⁺-containing sensory neurons were studied: P—peripheral domain; Cr—cranial domain; Cd—caudal domain; Cn—central domain of the DRG; Md—middle ganglion area. Section from the (a) proximal (b) middle and (c) distal part of the ganglion.

The PNx⁺-containing sensory nerve cells were present in all five ganglion domains: central (Cn), peripheral (P), cranial (Cr), caudal (Cd) and middle (Md). In both the left and the right ganglia, the vast majority of observed nerve cells were clustered in the Cn part of the ganglion ($29.1 \pm 6.2\%$ and $27.4 \pm 2.2\%$, respectively), while fewer PNx⁺ sensory neurons ($10.9 \pm 3.6\%$ and $12.1 \pm 5.3\%$) were observed in the P domain of the DRG. The rest of the PNx⁺ perikarya were dispersed quite evenly in the Md ($21.4 \pm 3.1\%$ and $21.5 \pm 0.9\%$), Cr ($19.7 \pm 1.5\%$ and $19.1 \pm 2.2\%$) and Cd ($18.9 \pm 1.3\%$ and $19.9 \pm 1.2\%$) domains of the ganglion. There were no statistically significant differences in the number of PNx⁺ nerve cells observed in the same domains of the left and the right DRG studied. Moreover, a similar intraganglionic distribution pattern of PNx⁺ neurons was observed in all the studied DRGs from the C, Th, L and S segments of the spinal cord. The details concerning the intraganglionic distribution pattern of PNx⁺ sensory neurons in particular domains of the left and the right DRGs are shown in Table 3.

Table 3. Intraganglionic distribution pattern of PN^X neuronal populations located in the bilateral DRGs in the C, Th, L and S segments of the spinal cord. The obtained data were pooled for each animal and are presented as mean ± SD (N = 6 animals).

DRG Subdomain	Segments of the Spinal Cord (%)							
	C		Th		L		S	
	Left	Right	Left	Right	Left	Right	Left	Right
P	15.1 ± 2.7	19.4 ± 2.1	12.1 ± 2.3	11.2 ± 1.8	10.7 ± 0.7	11.3 ± 2.0	11.3 ± 2.1	10.6 ± 1.3
Cr	20.9 ± 1.7	18.7 ± 1.2	20.4 ± 1.7	22.1 ± 1.6	20.1 ± 1.4	18.5 ± 3.8	20.4 ± 1.9	21.3 ± 4.2
Cd	17.3 ± 3.2	16.6 ± 1.5	17.4 ± 1.9	19.1 ± 2.4	19.2 ± 3.5	19.5 ± 1.9	18.1 ± 1.4	19.4 ± 4.1
Cn	24.2 ± 5.0	25.1 ± 3.9	26.1 ± 4.5	26.3 ± 1.8	27.9 ± 5.7	28.8 ± 4.5	31.1 ± 6.0	26.1 ± 6.7
Md	22.5 ± 1.5	20.2 ± 2.1	24.0 ± 1.3	21.3 ± 0.9	22.1 ± 5.8	21.9 ± 2.1	19.1 ± 1.9	22.6 ± 4.4

2.3. Immunohistochemical Characteristic of PN^X-Containing Perikarya in DRGs

A comprehensive analysis of double immunohistochemical staining showed the presence of PN^X-IR sensory nerve cells together with other biologically active substances like CGRP, SP, nNOS, GAL, CRT, PACAP, CART or SOM in all the studied DRGs.

2.3.1. PN^X/CGRP⁺ Nerve Cells

The largest subpopulation of PN^X DRG sensory nerve cells were neurons simultaneously containing CGRP (Figure 6a,b). Such cells accounted for 96.1 ± 0.8% of the total population of PN^X-IR neurons located in all the examined DRGs, while only a very small number of PN^X nerve cells (3.9 ± 0.8%) did not simultaneously express CGRP. The PN^X/CGRP⁺ neurons were observed in all the studied DRGs of the C, Th, L and S segments of the spinal cord (96.9 ± 3.3%; 95.1 ± 4.0%; 96.9 ± 2.7%; and 96.1 ± 3.2%, respectively). Statistically significant differences in the number of PN^X/CGRP⁺ neurons were not observed between selected DRGs of a given level of the spinal cord nor between DRGs from different spinal cord levels.

Regarding their diameter, the PN^X/CGRP-containing cells belonged to all three classes of afferent perikarya. The most numerous subpopulation of PN^X/CGRP⁺ neurons was that of SI-sized cells (69.2 ± 8.8%); the M-sized neurons were found to be distinctly less numerous (29.1 ± 8.3%), while Lg PN^X and CGRP-containing nerve cells (1.7 ± 0.5%) were rarely observed. No significant differences in the number of PN^X/CGRP⁺ DRG neurons belonging to the different size classes were observed between different levels of the spinal cord (Table 4).

Table 4. Relative frequency of different sizes (SI, M, Lg) of PN^X/CGRP⁺ perikarya found in DRGs of the C, Th, L and S spinal cord segments. The obtained data were pooled for each animal and are presented as mean ± SD (N = 6 animals).

Size of DRG Cells	Segments of the Spinal Cord (%)			
	C	Th	L	S
SI	57.1 ± 21.4	71.5 ± 4.9	73.3 ± 11.4	75.1 ± 6.7
M	42.10 ± 21.7	27.0 ± 4.9	26.1 ± 11.9	21.3 ± 3.2
Lg	0.8 ± 0.7	1.5 ± 0.6	0.6 ± 0.6	3.6 ± 3.6

The PN^X/CGRP⁺ sensory neurons were evenly dispersed in the individual DRG sections; a clear accumulation of these cells was observed in the Cn, Md, and Cr ganglion domains (25.3 ± 2.5%; 25.3 ± 0.7%; and 20.6 ± 1.3%, respectively), while a smaller number of PN^X/CGRP⁺ nerve cells was found in the Cd and the P parts (18.1 ± 1.8% and 10.7 ± 1.3%) of all the studied DRGs. The distribution pattern of the PN^X and CGRP-containing sensory neurons in the different domains of the DRGs are shown in Figure 7a.

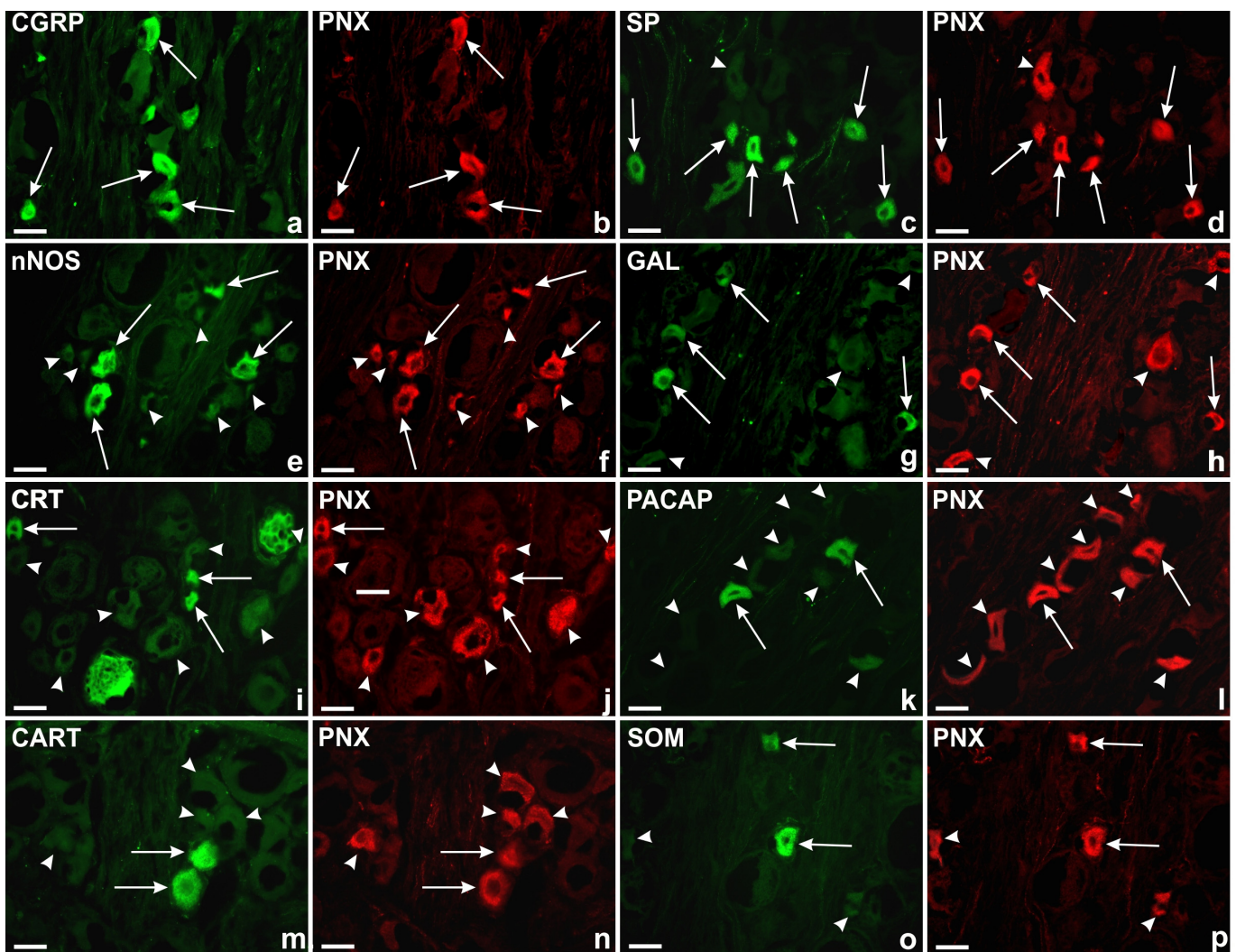


Figure 6. Representative images of the DRG sensory neurons. All the images were taken separately in green (fluorescein isothiocyanate—FITC) (a,c,e,g,i,k,m,o) and red (streptavidin—CY3) (b,d,f,h,j,l,n,p) fluorescent channels. Long arrows represent PNX⁺ cells (b,d,f,h,j,l,n,p) that simultaneously contain (a) calcitonin gene-related peptide (CGRP; 96.1%), (c) substance P (SP; 88.5%), (e) neuronal nitric oxide synthase (nNOS; 52.1%), (g) galanin (GAL; 20.7%), (i) calretinin (CRT; 10%), (k) pituitary adenylate cyclase-activating polypeptide (PACAP; 7.4%), (m) cocaine- and amphetamine-regulated transcript (CART; 5.1%), (o) somatostatin (SOM; 4.7%); arrowheads represent DRG PNX⁺ sensory nerve cells (d,f,h,j,l,n,p) which were simultaneously immunonegative for CGRP (a), SP (c), nNOS (e), GAL (g), CRT (i), PACAP (k), CART (m) and SOM (o). Scale bar: 50 μ m.

2.3.2. PNX⁺/SP⁺ Nerve Cells

The second most numerous subpopulation of PNX⁺ sensory neurons in the investigated DRGs was that containing SP (88.5 \pm 5.9%; Figure 6c,d), which was present in all the selected DRGs from the C, Th, L and S levels of the spinal cord (88.8 \pm 4.9%, 87.5 \pm 6.5%, 87.4 \pm 7.3% and 90.3 \pm 4.5%, respectively). No statistically significant differences were observed in the number of PNX⁺/SP⁺ sensory nerve cells between the selected DRGs in a given level of the spinal cord as well as between the different levels of the spinal cord.

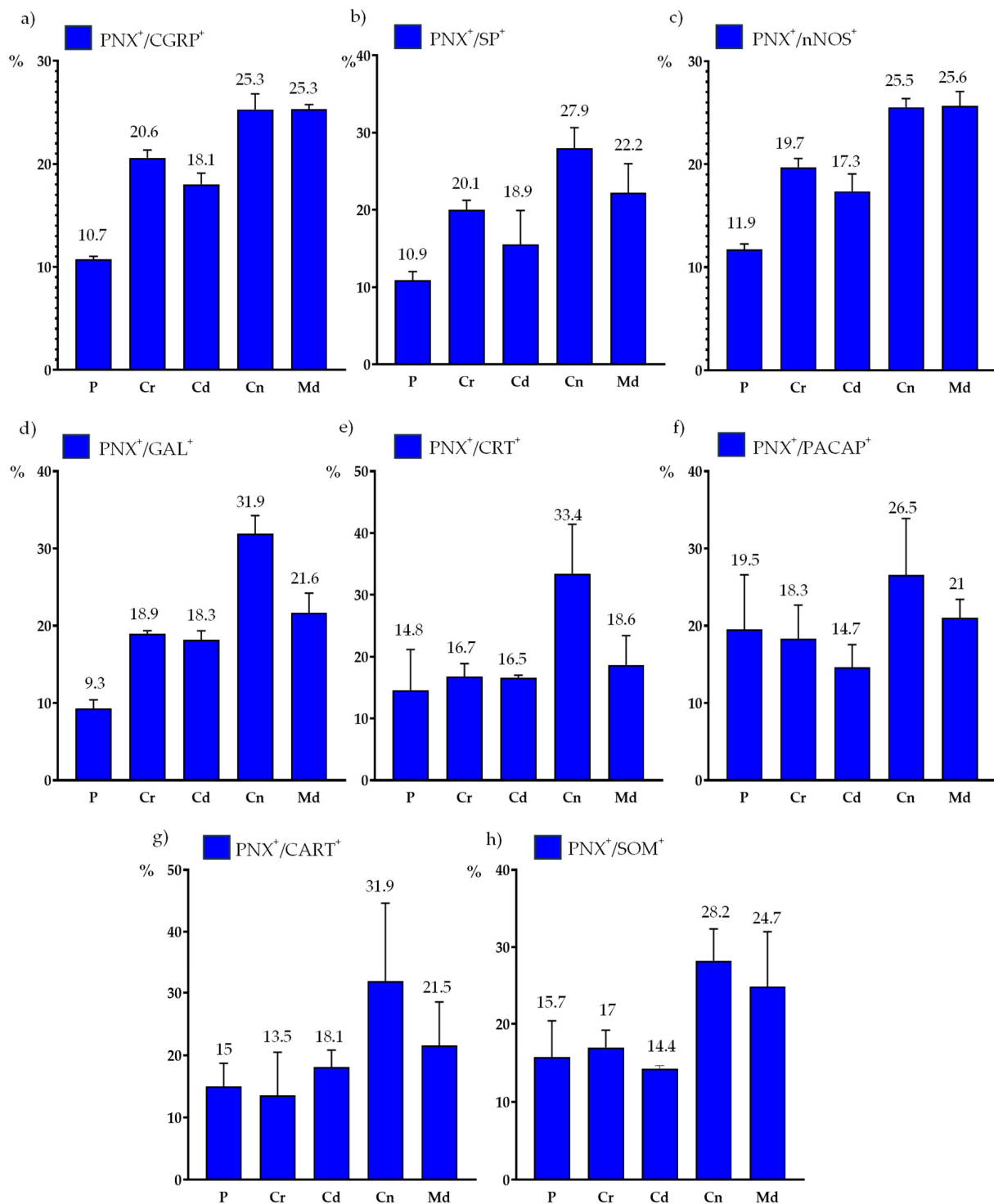


Figure 7. Distribution pattern of PNx⁺ neurons containing neurotransmitters in different domains (P, Cr, Cd, Cn and Md) of the DRG: (a) PNx⁺/CGRP⁺ sensory neurons, (b) PNx⁺/SP⁺ sensory neurons, (c) PNx⁺/nNOS⁺ sensory neurons, (d) PNx⁺/GAL⁺ sensory neurons, (e) PNx⁺/CRT⁺ sensory neurons, (f) PNx⁺/PACAP⁺ sensory neurons, (g) PNx⁺/CART⁺ sensory neurons, (h) PNx⁺/SOM⁺ sensory neurons. The obtained data were pooled for each animal and are presented as mean \pm SD (N = 6 animals).

In general, SP-IR was observed in all three size classes of PNx⁺ afferent perikarya, being present in $62.05 \pm 6.7\%$ of SI, $36.9 \pm 7.1\%$ of M and $1.05 \pm 0.4\%$ of Lg cells. There

were no significant differences in the number of PN^X⁺/SP⁺ DRG neurons representing the different size classes between the different levels of the spinal cord (for details, see Table 5).

Table 5. Relative frequency of different sizes of PN^X⁺/SP⁺ perikarya found in DRGs of the C, Th, L and S spinal cord segments. The obtained data were pooled for each animal and are presented as mean ± SD (N = 6 animals).

Size of DRG Cells	Segments of the Spinal Cord (%)			
	C	Th	L	S
Sl	53.4 ± 25.1	59.8 ± 11.2	67.3 ± 13.4	67.7 ± 11.7
M	45.9 ± 25.3	39.4 ± 11.8	31.2 ± 12.7	31.0 ± 11.0
Lg	0.7 ± 0.6	0.8 ± 0.6	1.5 ± 0.9	1.3 ± 0.7

Additionally, most of the PN^X⁺/SP⁺ neurons were unevenly distributed in different sensory ganglion domains. A clear accumulation of PN^X⁺ and SP-containing sensory nerve cells was found in the Cn, Md, Cr and Cd domains of the DRGs (27.9 ± 4.6%, 22.2 ± 6.5%, 20.1 ± 2.1% and 18.9 ± 7.6%, respectively). A smaller number of PN^X⁺/SP⁺ sensory neurons was found in the P part (10.9 ± 1.9%) of the studied DRGs. The distribution pattern of the PN^X⁺ and SP-containing sensory neurons in the different domains of the DRGs are shown in Figure 7b.

2.3.3. PN^X⁺/nNOS⁺ Nerve Cells

The third largest subpopulation of PN^X⁺ neurons in all the studied DRGs was that containing nNOS (52.1 ± 11.2%; Figure 6e,f). PN^X⁺/nNOS⁺ sensory nerve cells were observed in all the studied DRGs from the C, Th, L and S levels of the spinal cord (50.1 ± 16.5%, 56.9 ± 11.6%, 49.8 ± 7.0% and 51.7 ± 9.5%, respectively). No statistically significant differences in the numbers of PN^X⁺/nNOS⁺ neurons were observed between the selected DRGs of a given level of the spinal cord, nor between DRGs from different spinal cord levels.

In terms of their diameters, three classes of the PN^X⁺/nNOS⁺ DRG neurons were observed. The most numerous subpopulation was formed by M-sized cells (52.4 ± 6.6%) and a less numerous one by Sl-sized perikarya (46.1 ± 6.9%), while Lg PN^X⁺/nNOS⁺ neurons (1.5 ± 0.4%) were only observed sporadically. There were no significant differences in the number of PN^X⁺/nNOS⁺ DRG neurons representing different size classes between the different levels of the spinal cord (for details, see Table 6).

Table 6. Relative frequency of different sizes of PN^X⁺/nNOS⁺ perikarya found in DRGs of the C, Th, L and S spinal cord segments. The obtained data were pooled for each animal and are presented as mean ± SD (N = 6 animals).

Size of DRG Cells	Segments of the Spinal Cord (%)			
	C	Th	L	S
Sl	38.9 ± 15.2	43.4 ± 9.3	51.0 ± 3.4	50.9 ± 4.8
M	58.6 ± 15.1	56.1 ± 9.0	47.1 ± 4.6	47.9 ± 5.0
Lg	2.5 ± 3.3	0.5 ± 0.3	1.9 ± 1.2	1.2 ± 1.1

The PN^X⁺/nNOS⁺ sensory neurons were unevenly dispersed inside the ganglia, and were mainly clustered in the Md (25.6 ± 2.4%) and Cn (25.5 ± 1.4%) regions. The remaining nNOS-containing, PN^X⁺ nerve cells were present in the Cr, Cd and P (19.7 ± 1.4%, 17.3 ± 2.9% and 11.9 ± 0.9%, respectively) domains of the studied DRGs. The distribution pattern of PN^X⁺ and nNOS-containing sensory neurons in the different ganglionic domains is shown in Figure 7c.

2.3.4. PN^X/GAL⁺ Nerve Cells

The PN^X/GAL-containing cells constituted one of the smaller populations of DRG cells ($20.7 \pm 5.7\%$; Figure 6g,h), and were observed in all the studied DRGs from the C, Th, L and S spinal cord levels (constituting $16.1 \pm 5.3\%$, $18.7 \pm 7.7\%$, $22.8 \pm 4.9\%$ and $25.5 \pm 7.0\%$ of all cells, respectively). No statistically significant differences in the number of PN^X/GAL⁺ neurons were observed between the selected DRGs of a given level of the spinal cord, nor between DRGs from different spinal cord levels.

Regarding their diameter, the PN^X/GAL⁺ DRG cells belonged to only two classes of afferent perikarya: the most numerous subpopulation of SI-sized cells ($99.1 \pm 1.3\%$) and the distinctly less numerous subset of M-sized perikarya ($0.9 \pm 1.3\%$); PN^X/GAL⁺ Lg neurons were not found during the present study. There were no significant differences in the number of DRG neurons representing the different size classes between the different levels of the spinal cord (for details, see Table 7).

Table 7. The relative frequency of different sizes of PN^X/GAL⁺ perikarya found in DRGs of the C, Th, L and S spinal cord segments. The obtained data were pooled for each animal and are presented as mean \pm SD (N = 6 animals).

Size of DRG Cells	Segments of the Spinal Cord (%)			
	C	Th	L	S
SI	99.3 ± 1.0	97.3 ± 3.3	99.7 ± 0.5	100.0
M	0.7 ± 1.0	2.7 ± 3.3	0.3 ± 0.5	0.0
Lg	0.0	0.0	0.0	0.0

The largest accumulation of PN^X/GAL⁺ cells was observed in the Cn region of the studied DRGs ($31.9 \pm 4.1\%$), while the smallest number of these neurons was found in the P subdomain ($9.3 \pm 1.9\%$). The relative frequencies of the PN^X/GAL⁺ neurons were similar in the Md, Cr and Cd intraganglionic domains ($21.6 \pm 4.4\%$, $18.9 \pm 0.7\%$ and $18.3 \pm 1.9\%$, respectively). The distribution pattern of PN^X and GAL-containing sensory neurons in the different domains of the DRGs are shown in Figure 7d.

2.3.5. PN^X/CRT⁺ Nerve Cells

A colocalization study of PN^X with CRT unveiled the co-occurrence of these two biologically active substances in a small population ($10.05 \pm 1.6\%$; Figure 6i,j) of all the DRG cells studied. The PN^X/CRT⁺ sensory neurons were observed in all the selected DRGs from the C, Th, L and S levels of the spinal cord (constituting $11.2 \pm 1.3\%$, $11.2 \pm 4.9\%$, $10.5 \pm 6.0\%$ and $7.3 \pm 1.5\%$ of all cells, respectively). No statistically significant differences in the number of PN^X/CRT⁺ neurons were observed between the selected DRGs of a given level of the spinal cord, nor between DRGs from different spinal cord levels.

In terms of their diameter, three classes of PN^X/CRT⁺ DRG neurons were found. The vast majority of these cells were SI-sized neurons ($94.2 \pm 6.2\%$). In addition, a small number of M-sized PN^X/CRT⁺ sensory nerve cells ($5.1 \pm 6.3\%$) were observed, while Lg cells ($0.7 \pm 0.8\%$) were only occasionally present in the examined DRGs. While there were no significant differences in the number of PN^X/CRT⁺ neurons belonging to different size classes in the DRGs of the C, Th and L segments of the spinal cord, large PN^X/CRT⁺ neurons were not been observed in S DRGs (for details, see Table 8).

Table 8. The relative frequency of different sizes of PNX⁺/CRT⁺ perikarya found in DRGs of the C, Th, L and S spinal cord segments. The obtained data were pooled for each animal and are presented as mean \pm SD (N = 6 animals).

Size of DRG Cells	Segments of the Spinal Cord (%)			
	C	Th	L	S
Sl	80.3 \pm 2.6	98.1 \pm 3.3	98.9 \pm 1.9	99.5 \pm 0.8
M	17.2 \pm 2.5	1.8 \pm 3.1	1.0 \pm 1.7	0.5 \pm 0.8
Lg	2.5 \pm 4.1	0.1 \pm 0.2	0.1 \pm 0.1	0.0

The PNX⁺/CRT⁺ neurons were unevenly distributed between the different intraganglionic domains. The vast majority of PNX⁺ and CRT-containing sensory nerve cells were found in the Cn domain (33.4 \pm 3.8%), while smaller numbers of PNX⁺/CRT⁺ neurons were found in the Md, Cr, Cd and P subdomains (18.6 \pm 8.1%, 16.7 \pm 0.7%, 16.5 \pm 0.7% and 14.8 \pm 1.4%, respectively). The distribution pattern of the PNX⁺ and CRT-containing sensory neurons in the different domains of the DRGs are shown in Figure 7e.

2.3.6. PNX⁺/PACAP⁺ Nerve Cells

PACAP was found in 7.4 \pm 0.8% (Figure 6k,l) of all PNX-containing neurons and it was present in all the selected DRGs at the C, Th, L and S levels of the spinal cord (7.5 \pm 1.8%, 6.4 \pm 0.6%, 7.4 \pm 2.3% and 8.6 \pm 2.2%, respectively). No statistically significant differences in the number of PNX⁺/PACAP⁺ neurons were observed between the selected DRGs of a given level of the spinal cord, nor between DRGs from different spinal cord levels.

In general, PACAP-IR was observed in all three size classes of PNX⁺ afferent perikarya, being present in 87.2 \pm 4.5% of Sl, 12.1 \pm 4.0% of M and 0.7 \pm 0.6% of Lg cells. It should be stressed that statistically significant differences in the number of Sl- and M-sized PNX/PACAP-containing nerve cells were observed between the C and Th as well as the Th and S levels of the spinal cord. It should also be noted that the large PNX⁺/PACAP⁺ sensory neurons were only present in DRGs located in the C level of the spinal cord (see Table 9, Figure 8).

Table 9. Relative frequency of different sizes of PNX⁺/PACAP⁺ perikarya found in DRGs of the C, Th, L and S spinal cord segments. The obtained data were pooled for each animal and are presented as mean \pm SD (N = 6 animals); the data were statistically analyzed using the Student's two-tailed *t*-test for unpaired data and using one-way ANOVA with mean values compared using Tukey's multiple comparison test. Asterisks mark statistically significant differences: * *p* < 0.05, ** *p* = 0.005. The results were statistically analyzed using GraphPad PRISM 8.0 software.

Size of DRG Cells	Segments of the Spinal Cord (%)			
	C	Th	L	S
Sl	80.7 \pm 7.7 *	94.7 \pm 2.1 *,**	90.3 \pm 5.6	83.3 \pm 2.7 **
M	16.6 \pm 5.6 *	5.3 \pm 2.1 *,**	9.7 \pm 5.6	16.7 \pm 2.7 **
Lg	2.7 \pm 2.3	0.0	0.0	0.0

The PNX⁺/PACAP⁺ sensory neurons were dispersed throughout the ganglia, mainly in its Cn (26.5 \pm 2.6%) and Md (21.0 \pm 4.1%) regions. The remaining PACAP-containing, PNX⁺ nerve cells were present in the P, Cr and Cd domains of the studied DRGs (19.5 \pm 2.2%, 18.3 \pm 7.5% and 14.7 \pm 5.1%, respectively). The distribution pattern of the PNX⁺ and PACAP-containing sensory neurons in the different domains of the DRGs is shown in Figure 7f.

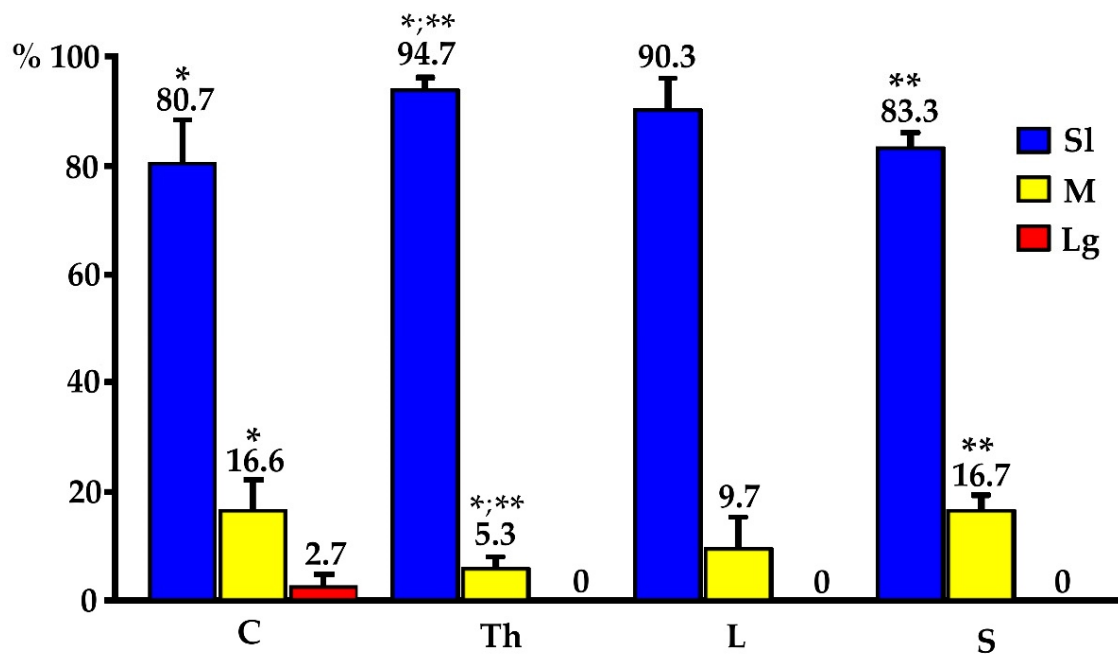


Figure 8. Relative frequency of different sizes of PNx⁺/PACAP⁺ perikarya found in DRGs of the C, Th, L and S spinal cord segments. The obtained data were pooled for each animal and are presented as mean \pm SD (N = 6 animals); the data were statistically analyzed using the Student's two-tailed *t*-test for unpaired data and using one-way ANOVA with mean values compared using Tukey's multiple comparison test. Asterisks mark statistically significant differences: * *p* < 0.05, ** *p* = 0.005. The results were statistically analyzed using GraphPad PRISM 8.0 software.

2.3.7. PNx⁺/CART⁺ Nerve Cells

Another small population of PNx⁺ DRG neurons contained CART (5.1 \pm 4.1%; Figure 6m,n), and were present in all the selected DRGs from the C, Th, L and S levels of the spinal cord (5.4 \pm 4.3%, 4.6 \pm 3.6%, 4.9 \pm 4.6% and 5.4 \pm 5.0%, respectively). No statistically significant differences in the number of PNx⁺/CART⁺ neurons were observed between the selected DRGs of a given level of the spinal cord, nor between DRGs from different spinal cord levels.

In general, CART-IR was observed in all three size classes of afferent perikarya, being present in 55.1 \pm 8.6% of M, 44.3 \pm 8.6% of SI and 0.6 \pm 11.5% of Lg cells. No significant differences in the size of PNx⁺/CART⁺ DRG neurons between different levels of the spinal cord were observed (see Table 10).

Table 10. The relative frequency of different sizes of PNx⁺/CART⁺ perikarya found in DRGs of the C, Th, L and S spinal cord segments. The obtained data were pooled for each animal and are presented as mean \pm SD (N = 6 animals).

Size of DRG Cells	Segments of the Spinal Cord (%)			
	C	Th	L	S
SI	20.4 \pm 6.2	66.6 \pm 2.8	41.1 \pm 5.5	49.2 \pm 2.7
M	79.6 \pm 6.2	33.4 \pm 2.8	56.4 \pm 1.0	50.8 \pm 2.7
Lg	0.0	0.0	2.5 \pm 1.4	0.0

Although the PNx⁺/CART⁺ sensory neurons were unevenly scattered throughout the individual ganglionic sections, a distinct accumulation of these cells was found in the Cn (31.9 \pm 22.02%) ganglionic domains, while a smaller number of PNx⁺/CART⁺ sensory neurons was found in the Md, Cd, P and Cr parts (21.5 \pm 12.1%, 18.1 \pm 4.7%, 15.0 \pm 6.4%

and $13.5 \pm 12.1\%$, respectively). The distribution pattern of the PNX⁺ and CART-containing sensory neurons in the different domains of the DRGs are shown in Figure 7g.

2.3.8. PNX⁺/SOM⁺ Nerve Cells

The SOM-containing sensory neurons constituted the smallest subpopulation ($4.7 \pm 2.5\%$; Figure 6o,p) of all PNX⁺ perikarya, being observed in all the investigated C, Th, L and S DRGs ($7.8 \pm 6.0\%$, $6.3 \pm 3.5\%$, $2.8 \pm 1.5\%$ and $2.1 \pm 0.9\%$, respectively). No statistically significant differences in the number of PNX⁺/SOM⁺ neurons were observed between selected DRGs of a given level of the spinal cord, nor between DRGs from different spinal cord levels.

In terms of their diameter, three classes of the PNX⁺/SOM⁺ DRG neurons were observed. The most numerous subpopulation was SI-sized cells ($85.2 \pm 9.4\%$) with a distinctly less numerous subset of M-sized perikarya ($14.6 \pm 5.3\%$), while the Lg PNX⁺/SOM⁺ neurons ($0.2 \pm 1.1\%$) were found sporadically in all the DRGs studied. There were no significant differences in the number of PNX⁺/SOM⁺ DRG neurons representing different size classes between the different levels of the spinal cord; however, it should be noted that Lg sensory neurons were not been observed in this subpopulation of PNX⁺ nerve cells in both the C and S ganglia of the spinal cord (for details, see Table 11).

Table 11. The relative frequency of different sizes of PNX⁺/SOM⁺ perikarya found in DRGs of the C, Th, L and S spinal cord segments. The obtained data were pooled for each animal and are presented as mean \pm SD (N = 6 animals).

Size of DRG Cells	Segments of the Spinal Cord (%)			
	C	Th	L	S
SI	82.5 ± 2.1	81.9 ± 2.3	86.9 ± 4.5	89.6 ± 9.0
M	17.5 ± 2.1	17.7 ± 1.7	12.8 ± 2.0	10.4 ± 9.0
Lg	0.0	0.4 ± 0.5	0.3 ± 1.8	0.0

A distinct accumulation of PNX-labeled and SOM⁺ cells was found in the Cn ($28.2 \pm 7.1\%$) and Md ganglionic regions ($24.7 \pm 2.5\%$), while these cells were less numerous in the Cr, P and Cd parts of the ganglia ($17.0 \pm 3.8\%$, $15.7 \pm 8.1\%$ and $14.4 \pm 0.7\%$, respectively). The distribution pattern of the PNX⁺ and SOM-containing sensory neurons in the different domains of the DRGs are shown in Figure 7h.

3. Discussion

PNX is a newly identified peptide that, in the rat brain, is highly expressed in the hypothalamus, medial division of the central amygdaloid nucleus, the spinal trigeminal tract of the medulla and the spinocerebellar tract [11]. Moreover, enzyme immunoassays also detected a high level of PNX (>4.5 ng/g of tissue) in the spinal cords of rats [5]. Immunohistochemical studies in rat also revealed the presence of PNX in trigeminal ganglia, as well as in ganglia comprising neurons projecting to the superficial layers of the spinal cord, such as the DRGs and nodose ganglia [5]. These projections may belong to A δ -terminals—thin, myelinated fibers capable of responding to both thermal and mechanical stimuli—or to C-fibers, which are unmyelinated, slow-conducting axons that can, due to their high activation threshold, detect painful stimuli. Both of these types of NFs are assigned to nociceptors as they respond to destructive, thermal, mechanical or chemical stimuli [12]. Furthermore, PNX⁺ afferent NFs targeting the spinal cord were revealed in mice and pigs and were present in all spinal cord segments at equal levels [6,13], whereas PNX was observed mainly in NFs located in the superficial DH layer, in laminae I and II [5,6]. It is also worth noting that PNX-IR NFs participate in skin innervation in rodents: subcutaneous injections of the fluorescent retrograde tracer Fluorogold labeled a population of DRG cells, some of which also contained PNX, thus raising the possibility that PNX

released from these terminals could affect other sensory NF/sensory signaling pattern from the skin to the spinal cord [13].

In addition, the presence of “true” PNX was confirmed by the use of mass spectrometry (not only by showing that the major peak corresponds to the peptide, but also by verifying its presence using the fragmentation spectra of its individual amino acids) in the extracts of DRG cells (present study) as well as in the spinal cord (both rat [5] and mouse [13]).

The available literature implicates PNX in pain transmission, and it has been found that the intrathecal injection of amidated PNX suppresses visceral pain; however, it did not affect thermal pain sensation [5]. Moreover, PNX’s contribution to sensory modulation is also supported by its participation in inducing the itching effect, as revealed in a study by Cowan and colleagues [13].

To date, the presence of PNX in DRG neurons has only been studied in rodents [5,13]. Thus, for the first time, our study demonstrated the presence of PNX in afferent neurons of porcine DRGs. We have found that PNX⁺ neurons accounted for a relatively large subpopulation (approximately 20% of all cells) in all DRGs of each segment of the spinal cord. Furthermore, considering the differences in the size (diameter) of the PNX-containing cells, it was demonstrated that the vast majority of PNX-IR neurons were S1-sized neurons (average diameter up to 40 μm). M-sized cells (40–70 μm) were distinctly less numerous, while Lg PNX⁺ cells (diameter > 71 μm) were only occasionally observed. This finding appears to be inconsistent with the previous results described in rodents, where many of the PNX⁺ neurons belonged to the M-sized DRG perikarya [5]. As there is a consensus that the size of the sensory cell is associated with different “physiological functional classes”, the data presented above may suggest a different involvement of PNX-positive cells in sensory modalities in rodents and the domestic pig. However, this hypothesis requires further verification.

The present study, for the first time, also focused on the immunohistochemical characteristics of PNX⁺ DRG neurons. We examined PNX colocalization patterns with several neurotransmitters/their markers that were previously revealed in DRG neurons, with particular attention to those biologically active molecules that were previously described in S1- and/or M-diameter afferent cells: CGRP, SP, nNOS, GAL, CRT, PACAP, CART and SOM [14,15].

Previous studies revealed that, CGRP, together with SP (see below), appears to be the “canonical” transmission molecule of afferent neurons in all mammalian species studied so far (human, horse, dromedary camel, pig, cat, rat and mouse) [16–20]. According to the available data, the proportion of sensory neurons containing CGRP (or expressing mRNA encoding this peptide [21,22]) ranging, on average, between 50 and 60% of all DRG cells, regardless of the species studied. Furthermore, their axonal processes constitute the largest population of nerve fibers forming not only individual laminae of the dorsal horns of the spinal cord (especially laminae I–III, V and X), but also Lissauer’s tract [17]. Interestingly, this pattern of intraspinal distribution of CGRP-positive central projections of DRG cells persists in all spinal cord neuromeres, which is most prominent in the thoracic ones [16].

In addition to being involved in the conduction of sensory and pain stimuli in a wide variety of mammals, including human [17,18,23–25], CGRP is also known to be a very potent vasodilator [26] and a deficiency in CGRP release is related to a lack of a vasodilation reflex [27]; thus, blockade of CGRP secretion exerts an analgesic effect in people suffering from migraine [28].

However, CGRP, along with SP, released from the terminals of DRG neurons in response to noxious mechanical, chemical or thermal stimuli [29] may also contribute to the development and maintenance of neurogenic inflammation: CGRP acts as an extremely potent vasodilator [30] while SP, acting on neurokinin 1 (NK1) receptors, evokes increased vascular permeability [31]. Therefore, it can be concluded that the intensified secretion of these peptides may contribute to the formation of edema, increased blood flow and the influx of inflammatory cells at the site of inflammation.

The above-mentioned close interdependence and cooperation of CGRP and SP in numerous regulatory loops seem to result from the fact that both substances coexist very often in the same sensor cell [14,17,20] from which they are released together and synergistically interact with target cells, supporting each other. For example, as revealed by Biella and co-workers [32], the excitatory effects of SP arising from spontaneous and noxious activity were significantly enhanced by CGRP in rats. Although the mechanism by which CGRP may potentiate the effects of SP is not fully clear, there is evidence that CGRP may delay the enzymatic degradation of SP [33,34]. CGRP has also been reported to increase the release of SP [35] as well as the excitatory amino acid transmitters glutamate and aspartate [36] from central terminals of DRG neurons, possibly leading to the strengthening of synaptic connections in the spinal dorsal horn, as well as increasing the effectiveness of these substances on the peripheral targets (for details, see [37]).

The second largest population of PNX⁺ DRG cells observed in this study were SP-containing neurons, accounting for approximately 89% of all PNX⁺ afferent cells. This observation seems to be in stark contrast to the data obtained in studies of the co-occurrence of PNX and SP in mouse DRG cells, where both neurotransmitters were present in separate cell subpopulations [5]. Therefore, it seems reasonable to hypothesize that PNX is probably involved in regulating different functions of DRG sensory cells in both species.

As shortly mentioned above, SP, like CGRP, is primarily considered a transmitter of sensory and pain stimuli, the presence of which has been shown in DRG cells in every species studied so far, including humans [38–41]. So far, studies on the presence and distribution patterns of SP⁺ cells in the DRGs of the domestic pig have shown the presence of cells containing this tachykinin, especially in subpopulations of SI- and M-sized neurons. Moreover, there is irrefutable evidence that SP occurs in both the somatic as well as visceral subclasses of these perikarya [14,42]. This is consistent with the data obtained in other species studied so far, including humans [21], guinea pigs [39], mice [5] and rats [43,44], with regard to both the number of chemically encoded afferent cells and their classification into individual size classes.

While the co-existence of PNX with CGRP in the studied porcine DRG cells was shown in a very high percentage of cells (approximately 96% of all PNX⁺ cells), only slightly more than half of the CGRP⁺ cells (56%) also contained PNX. Moreover, a very similar picture emerged from the studies on the co-occurrence pattern of PNX and SP performed in this study: almost 90% (exactly 88.5%) of all PNX⁺ cells contained SP, and approximately 50% of all SP⁺ cells were also PNX-positive. The co-localization of both peptides was observed mainly in SI- and M-sized ganglion cells.

Thus, based on the comparison of the relative numbers of DRG cells containing the individual transmitters, there is no mathematical possibility that all three peptides do not co-occur in at least approximately 80–85% of all PNX⁺ cells. This suggestion is further, although indirectly, supported by the observation of the high degree of co-occurrence of PNX with SP and/or CGRP in the axonal fibers of DRG cells forming the dorsal horn laminae of the porcine spinal cord [6].

Moreover, considering the degree of co-localization of PNX and nNOS in DRG cells (approximately 50% of all PNX⁺ cells; see below), it seems that neurons containing all four transmitting substances must also be present in at least 30% of all the porcine DRG cells. Unfortunately, at present, insufficient knowledge of the possible functions of PNX in peripheral sensory pathways prevents us from suggesting its physiological significance, either in the case of hypothetical PNX⁺/CGRP⁺/SP⁺ cells or in the population of cells additionally co-expressing nNOS.

nNOS is a marker of the nitergic subpopulation of afferent cells that are involved in the regulation of numerous physiological processes in the peripheral and central nervous systems. Nitric oxide (NO), produced by nNOS, is an important neurotransmitter in the periphery, mainly in the control of, among others, neuronal plasticity [45], neurogenesis [46], neuroprotection [47] as well as modulation of nociceptive transmission in neuropathic

pain [48] and it is believed that inhibition of nNOS may be a valuable strategy in the treatment of not only neuropathic pain [49] but also several other illnesses [50].

In the present study, PNX⁺/nNOS-containing neurons formed the third largest (approximately 50%) population among all afferent cells capable of synthesizing and releasing PNX as their transmitter; the vast majority of these neurons were SI- and M-sized cells. This is well in line with the data obtained in other species (humans, rats, mice, sheep, dromedary camels [20,51–53]) where nitrenergic afferent neurons were found in an average of 40–50% of all DRG cells, with the highest percentage in the subpopulation of SI- and M-sized neurons. It should be emphasized that the high degree of nNOS co-localization with SP and CGRP, reported by Russo and colleagues [53], additionally supports the above hypothesis, suggesting the existence of a PNX⁺/SP⁺/CGRP⁺/NOS⁺ population of DRG cells.

The co-existence of PNX and GAL was found exclusively in porcine DRGs in approximately one-fifth (20.7%) of SI-sized neurons. As neither the immunoreactivity to GAL alone nor the co-occurrence of PNX and GAL immunoreactivities was observed in M- or Lg-sized cells, this strongly suggests the involvement of cells containing these two peptides in the regulation of nociceptive activities in the domestic pig. This suggestion corresponds well with the data from studies in other species, especially rats: GAL was also found in SI-sized DRG cells in rodents (in a few cells [54]) and humans (approximately 12% [22]); moreover, it has also been observed that their number increases dramatically after peripheral nerve damage [55,56]. Numerous studies indicate that GAL may reduce the perception and transmission of pain by increasing the pain threshold as a result of increasing K⁺ conductance or decreasing Ca²⁺ conductance in the brain, spinal cord and peripheral neurons [57,58]. Moreover, in behavioral studies, it was found that reducing the effect of GAL leads to an increase in neuropathic pain-like behaviors and, on the contrary, the upregulation of GAL leads to a decrease in neuropathic pain in animal models [56].

In contrast to its co-occurrence pattern with CGRP, SP or GAL, PNX co-localized with the other studied substances (neuropeptides: PACAP, CART and SOM; calcium-binding protein: CRT) in only a relatively few porcine DRG cells.

In the case of the co-occurrence of PNX and PACAP, a significantly lower degree of colocalization was observed in this study (about 7% of all PNX⁺ cells simultaneously contained PACAP); at the same time, however, it should be emphasized that the vast majority of neurons chemically coded by the presence of both peptides belonged to the population of small, probably nociceptive, neurons. These observations agree fairly well with the data obtained in rodents, where PACAP⁺ cells were part of a SI-diameter neuronal population [59,60]. It should be noted, however, that the number of PACAP⁺ cells in rat DRGs was slightly higher, reaching approximately 10–17.5% of all sensory nerve cells [61], suggesting interspecies differences.

It is worth noting that both PACAP and GAL are dramatically up-regulated in damaged DRG cells (up to 75% in the rat [60]), especially in SI-sized cells (probably nociceptive perikarya), and act as neuroprotective and/or pro-regenerative peptides in this scenario [62–64]. Unfortunately, so far, there are no data on the possible functions of PNX in these regulatory mechanisms, and therefore the question of the possible existence of a subpopulation of PNX⁺/GAL⁺/PACAP⁺ cells, as well as their presumed targets and possible regulatory functions remains open and requires further, more detailed research.

In contrast to the patterns of PNX co-localization with the other biologically active agents discussed above, where the vast majority of observed PNX⁺ cells belonged almost exclusively to SI- or M-diameter cells, PNX and CART co-localization was observed in the pig in all three neuronal size classes, with the M-sized PNX⁺/CART⁺ cells being the most numerous. While the data on the presence of CART in porcine DRG cells collected in this study appear to be in full agreement with the results obtained by Zacharko-Siembida and colleagues [65] in the lumbar porcine DRGs (in both studies, the relative number of CART⁺ cells oscillated around 5% of all DRG cells), a slightly more numerous (approximately 10%) population was observed in rodents [66]. Remarkably, Zacharko-Siembida and colleagues

found that the vast majority (approximately 70%) of porcine CART⁺ DRG cells simultaneously contain CGRP. This allows for the assumption that some of the sensory cells may also contain, in addition to PNX⁺/CGRP⁺/SP⁺/NOS⁺, CART, which additionally suggests the need for in-depth research on both the chemistry and the functional significance of these sensory cells.

The last of the neuropeptides whose pattern of co-occurrence with PNX was the subject of interest in this work was SOM, a substance present in both the pig and the rat [67] in a small (up to 10%) subpopulation of the DRG cells. It has been shown that a small fraction (about 6% of all PNX⁺ cells) also contains SOM, which, in the light of the available literature data (both PNX and SOM are implicated as transmitters subserving the itch conduction pathway [13,68,69]) the most recent data, see [70], suggests that these cells are representatives of pruriceptors. However, further studies are needed to unveil the exact relevance of PNX in this neural modality.

Intracellular calcium-binding proteins may play an important role in the nociceptive excitability of neurons [71,72], as well as in proprioception [73], as evidenced by the presence of calbindin (CB) in excitatory interneurons within the superficial DH [74]. Taking this into account, we decided to analyze the co-occurrence of CRT (protein closely related to the above-mentioned CB) with PNX in porcine primary afferent cells. It was found that PNX coexisted with CRT in a relatively small population of DRG neurons (approximately 10.5% of all PNX-containing cells), due to the fact that CRT was expressed mainly in Lg-sized neurons, and the vast majority of PNX⁺ neurons were small-sized cells. These data are in line with reports emerging from studies concerning the CB or CRT expression patterns in rats and fowl [15,73,75], which showed that the vast majority of CB- or CRT-positive neurons were M to Lg in size [73].

Limitations of the Study

The most important limitation of the present study was the inability to perform simultaneous colocalization studies of a larger number of neurotransmitters in the same nerve cell, due to the unavailability of appropriate primary and/or secondary antibodies. Similarly, the authors are aware that the value of this work would be higher if it were possible to demonstrate expression patterns of membrane/cytosolic receptor subtypes specific to the studied neurotransmitters; unfortunately, as in the case of studies based on multiple colocalizations in a single afferent cell, the unavailability of antibodies recognizing the mentioned receptors was an obstacle. The last limitation was the inability to link the observed PNX⁺ cell subtypes with their target tissues within the assumptions of this study: an analysis of the presence of PNX⁺ cells in the DRGs of so many spinal cord neuromeres would require the injection of a retrograde neuronal tracer into individual internal organs in such a large number that the planned experiment was simply becoming impossible. On the other hand, the use of an anterograde tracing technique was excluded due to the need to inject the tracer directly into the studied DRG, which would certainly cause changes in the expression pattern(s) of the tested substances.

4. Materials and Methods

4.1. Experimental Animals

The investigations were performed on 6 juvenile female pigs (8–12 weeks old, 15–20 kg body weight—b.w.) of the Large White Polish breed. The animals were kept under standard laboratory conditions. They were fed standard fodder (Grower Plus, Wipasz, Wadąg, Poland) and had free access to water. All surgical procedures were performed following the rules of the local Ethics Commission (affiliated with the National Ethics Commission for Animal Experimentation, Polish Ministry of Science and Higher Education; decision No. 40/2020 from 22 July 2020).

4.2. Surgical Procedures

All animals were pretreated with atropine (Polfa, Warsaw, Poland; 0.05 mg/kg b.w., subcutaneous (s.c.) injection) and azaperone (Stresnil, Janssen Pharmaceutica, Belgium; 2.5 mg/kg b.w., intramuscular (i.m) injection) and after thirty minutes, they were deeply anesthetized with sodium pentobarbital (Tiopental, Sandoz, Poland; 0.5 g per animal, administered according to the effect). The 5th lumbar DRGs (L5) were collected intra-operatively from 3 out of 6 pigs, and they were used for PNx identification using mass spectroscopy (MS). Next, the anesthesia was deepened, and after cessation of breathing, all the animals were transcardially perfused with freshly prepared 4% paraformaldehyde in 0.1 M phosphate buffer (pH 7.4). Whole spinal cords, including the attached DRGs, were gently dissected, sectioned into individual neuromeres (assuming the anatomical extent of their *fila radicularia* as boundaries) and each neuromere was fixed in the same fixative (10 min at room temperature), washed several times in 0.1 M phosphate buffer (pH 7.4; 4 °C; twice daily for three days) and stored in 18% buffered sucrose at 4 °C (for two weeks) until sectioned.

4.3. Protein Extraction

The proteomics analysis of the DRGs was performed at the Mass Spectrometry Laboratory at the Institute of Biochemistry and Biophysics of the Polish Academy of Sciences. The tissue was transferred to 2 mL tubes containing a mix of 1.4 mm, 2.8 mm and 5.0 mm zirconium oxide beads. The lysis was performed in 500 µL of 25% trifluoroethanol (TFE) in 100 mM triethylammonium bicarbonate buffer (TEAB). The tissue was lysed using a Precellys Evolution homogenizer (Bertin Technologies, Montigny-le-Bretonneux, France) using 6 rounds of a program with the following parameters: 10 cycles of 6800 rpm for 60 s with a 20 s pause in between. Homogenization was performed at 4 °C with dry ice cooling. After lysis, the samples were centrifuged (14,000 × *g*, 30 min, 4 °C) and transferred to 1.5 mL tubes with low retention. Cysteine residues were reduced by incubation with 10 mM Tris (2-carboxyethyl)phosphine (TCEP) for 60 min, followed by blocking with 25 mM chloroacetamide. A 100 µL volume of the lysate was diluted to 500 µL with a 10% aqueous solution of acetonitrile (ACN), vortexed and briefly spun to remove the precipitated proteins. The sample was transferred to a 30 kDa cut-off filter (Vivacon 500, Sartorius, Göttingen, Germany). After centrifugation (14,000 × *g*, 2 h, 25 °C), the filtrate was transferred to a new Eppendorf tube, dried in a SpeedVac and reconstituted in 40 µL of 0.1% formic acid.

4.4. Mass Spectroscopy (MS)

The samples were analyzed using a liquid chromatography–mass spectrometry (LC-MS) system composed of Evosep One (Evosep Biosystems, Odense, Denmark) coupled to an Orbitrap Exploris 480 mass spectrometer (Thermo Fisher Scientific, Bremen, Germany). A 20 µL volume of the sample was loaded onto disposable Evotips C18 trap columns as described previously [11]. Chromatography was carried out at a flow rate of 250 nl/min using the 88 min (15 samples per day) preformed gradient on N EV1106 analytical column (Dr Maisch C18 AQ, 1.9 µm beads, 150 µm ID, 15 cm long; Evosep Biosystems, Odense, Denmark). Data were acquired in positive mode with a data-dependent method using the following parameters: MS1 resolution was set at 120 000 with a 500% normalized automatic gain control (AGC) target, auto maximum inject time and a scan range of 250 to 1200 *m/z*; cycle time was set to 1 s. The ions with an *m/z* corresponding to the PNx protein with amidation within 1.6 *m/z* window were subjected to fragmentation with a normalized collision energy of 30%. For MS2, the resolution was set at 30,000 with a 1000% normalized AGC target and auto maximum inject time. The spray voltage was set at 2.1 kV, the funnel radio frequency (RF) level at 40, and the heated capillary temperature at 275 °C.

4.5. MS Data Analysis

Protein identification was performed using the Proteome Discoverer software suite (version 2.4.0.305) and the Sus scrofa full Uniprot database (version 2022_02). The search

included non-cleaved proteins, Carboamidomethylation (C) was set as a fixed modification and Oxidation (M) and Amidation on Protein C-term were set as a variable ones. Fixed Value PSM (peptide-spectra match) Validator was used for PSM validation. At the consensus step, the basic Proteome Discoverer settings were used.

4.6. Sectioning of the Tissue Samples

Three representative DRGs from each level of the spinal cord were selected for this study. Bilateral DRGs from cervical (C: C1, C4, C7), thoracic (Th: Th1, Th7, Th15), lumbar (L: L1, L3, L6) and sacral (S: S1, S3) neuromeres were located pairwise on a pre-cooled block of the optimal cutting temperature compound medium (OCT) in a manner that allowed for the easy determination of the position of individual subdomains of the DRG sections under a microscope. Frozen ganglia were cut with an HM525 Zeiss freezing microtome into transverse 10 μm thick serial sections (four sections on each slide) and mounted on chrome alum–gelatine-coated slides.

4.7. Immunohistochemical Procedure and Estimation of the Total Number of PNX-Containing DRG Neurons

Serial 10 μm thick DRG sections were processed for double-labeling immunofluorescence (following a previously described protocol [14]) using combinations of primary immunosera raised in different species. After immersion of the tissues in a blocking solution containing 0.1% bovine serum albumin, 1% Triton X 100, 0.01% sodium azide (NaN_3), 0.05% thimerosal and 10% normal goat serum in 0.01 M phosphate-buffered saline (PBS) for 1 h at room temperature to reduce non-specific background staining, the sections were repeatedly rinsed in PBS, and then incubated overnight at room temperature with PNX antiserum applied in a mixture with antisera against: CART, CGRP, CRT, GAL, nNOS, PACAP, SOM and SP. A combination of antisera against PNX and protein gene product 9.5 (PGP 9.5) was used to accurately determine the distribution pattern and the total number of PNX cells in the right and left DRGs from the different levels of the spinal cord (C, Th, L and S). Primary antisera were visualized by fluorescein isothiocyanate (FITC)-conjugated rat, guinea pig or mouse immunoglobulin G (IgG)-specific secondary antisera or streptavidin (CY3) rabbit-specific antiserum (Table 12). After rinsing the tissue with PBS, Fluoromount™ Aqueous Mounting Medium (Sigma Aldrich, Saint Louis, MO, USA, F4680) was applied to the section and then the tissue was covered with a coverslip.

PNX/PGP 9.5-positive perikarya were counted in every fourth section of six slides per DRG studied, while the colocalization of PNX with other biologically active substances was assessed from three slides (one section on the given slide for colocalization experiment) taken symmetrically from each one-third (anterior, middle, posterior; total = 9 slides) of each DRG studied: C (C1, C4, C7), Th (Th1, Th7, Th15), L (L1, L3, L6) and S (S1, S3). While the number of DRG cells belonging to specific neuronal subpopulations was manually counted within the entire section of the ganglion being assessed (only neuronal profiles in which the cell nucleus was clearly visible were counted), the diameters of PNX-positive (PNX^+) perikarya were measured using a subroutine of the image analysis software (AnalySIS version 3.0, Soft Imaging System GmbH, Germany). The neurons were divided into three size classes: S1 (average diameter up to 40 μm), M (diameter 41–70 μm) and Lg (diameter ≥ 71 μm). To determine the relative frequency of the appropriately chemically coded subpopulation of the studied sensory neurons, all profiles of cells containing, for example, CGRP (visualized with FITC-labeled secondary antibody) and PNX (visualized with CY3-labeled secondary biotinylated antibody) were counted within the examined DRG section. The correctness of the assessment was confirmed using a special filter allowing the simultaneous observation of FITC and CY3 excitation. The combinations of primary antibodies employed in this study for double labeling are presented in Table 13.

Table 12. List of primary antisera and secondary reagents used in the study: CART, CGRP, CRT, GAL, nNOS, PACAP, protein gene product 9.5 (PGP 9.5), PNX, SOM, SP, FITC, CY3.

Antigen	Code	Dilution	Host	Supplier
Primary antibodies				
CART	MAB 163	1:1000	Mouse	R&D Systems, Wiesbaden, Germany
CGRP	T-5027	1:800	Guinea pig	Peninsula Laboratories, San Carlos, CA, USA
CRT	6B3	1:2000	Mouse	SWANT, Burgdorf, Switzerland
GAL	T-5036	1:1500	Guinea pig	Peninsula Laboratories, San Carlos, CA, USA
nNOS	N2280	1:200	Mouse	Sigma-Aldrich, St. Louis, MO, USA
PACAP	T-5039	1:1000	Guinea pig	Peninsula Laboratories, San Carlos, CA, USA
PGP 9.5	7863-2004	1:5000	Mouse	Biogenesis, Poole, UK,
PNX	H-079-01	1:7000	Rabbit	Phoenix Pharmaceuticals Inc., Burlingame, CA, USA,
SOM	MAB 354	1:50	Rat	Merck Millipore, Temecula, CA, USA
SP	8450-0004	1:200	Rat	Bio-Rad, Kidlington, UK
Secondary reagents				
CY3-conjugated anti-rabbit	711-166-152	1:700	Donkey	Jackson I.R.; West Grove, PA, USA, Baltimore Pike
FITC-conjugated anti-mouse IgG	715-096-151	1:800	Donkey	Jackson I.R.; West Grove, PA, USA, Baltimore Pike
FITC-conjugated anti-guinea pig IgG	706-095-148	1:800	Donkey	Jackson I.R.; West Grove, PA, USA, Baltimore Pike
FITC-conjugated anti-rat IgG	712-095-153	1:400	Donkey	Jackson I.R.; West Grove, PA, USA, Baltimore Pike

Table 13. Double staining combinations employed in this study.

Primary Antibody	Primary Antibody	Secondary Antibody
PNX (rabbit)	CART (mouse)	CY3 (rabbit), FITC (mouse)
PNX (rabbit)	CGRP (guinea pig)	CY3 (rabbit), FITC (guinea pig)
PNX (rabbit)	CRT (mouse)	CY3 (rabbit), FITC (mouse)
PNX (rabbit)	GAL (guinea pig)	CY3 (rabbit), FITC (guinea pig)
PNX (rabbit)	nNOS (mouse)	CY3 (rabbit), FITC (mouse)
PNX (rabbit)	PACAP (guinea pig)	CY3 (rabbit), FITC (guinea pig)
PNX (rabbit)	PGP (mouse)	CY3 (rabbit), FITC (mouse)
PNX (rabbit)	SOM (rat)	CY3 (rabbit), FITC (rat)
PNX (rabbit)	SP (rat)	CY3 (rabbit), FITC (rat)

The labeled sections were viewed using an Olympus BX61 microscope (Olympus, Hamburg, Germany) equipped with an appropriate filter set for CY3 and FITC. Micrographs were taken using an Olympus XM10 digital camera (Tokyo, Japan). The microscope was equipped with cellSens Dimension 1.7 Image Processing software (Olympus Soft Imaging Solutions, Münster, Germany). Finally, the obtained data were pooled for each animal and are presented as mean \pm SD and were statistically analyzed using the Student's two-tailed *t*-test for unpaired data and one-way ANOVA with mean values compared using Tukey's multiple comparison test. The results were statistically analyzed using GraphPad PRISM 8.0 software (GraphPad Software, La Jolla, CA, USA). The differences were considered to be significant at $p < 0.05$.

4.8. Control of Specificity of Immunohistochemical Procedures

Standard controls, i.e., preabsorption for the neuropeptide antisera (20 μ g of appropriate antigen per 1 mL of the corresponding antibody at working dilution; all antigens were purchased from Peninsula (San Carlos, CA, USA), R&D Systems (Wiesbaden, Germany), SWANT (Burgdorf, Switzerland), Sigma, Phoenix (Burlingame, CA, USA)—Table 14), as well as omission and replacement of the respective primary antiserum with the correspond-

ing non-immune serum completely abolished immunofluorescence and eliminated the specific staining. Photos showing the preabsorption controls are presented in Figure 9.

Table 14. List of antigens used in pre-absorption test.

Antigen	Code	Dilution	Supplier
CART	MAB0041	1:1000	R&D Systems, Germany
CGRP	T-4030	1:800	Peninsula Laboratories, San Carlos, CA, USA
CRT	6-His human calretinin (recombinant) Lot No.: 22	1:2000	SWANT, Switzerland
GAL	T-4862	1:1500	Peninsula Laboratories, San Carlos, CA, USA
nNOS	N3033	1:200	Sigma, St. Louis, MO, USA
PACAP	A9808	1:1000	Sigma, St. Louis, MO, USA
PNX	079-01	1:7000	Phoenix Pharmaceuticals Inc.; Burlingame; Kalifornia; San Carlos, CA, USA
SOM	S9129	1:50	Sigma-Aldrich, St. Louis, MO, USA
SP	S6883	1:200	Sigma-Aldrich, St. Louis, MO, USA

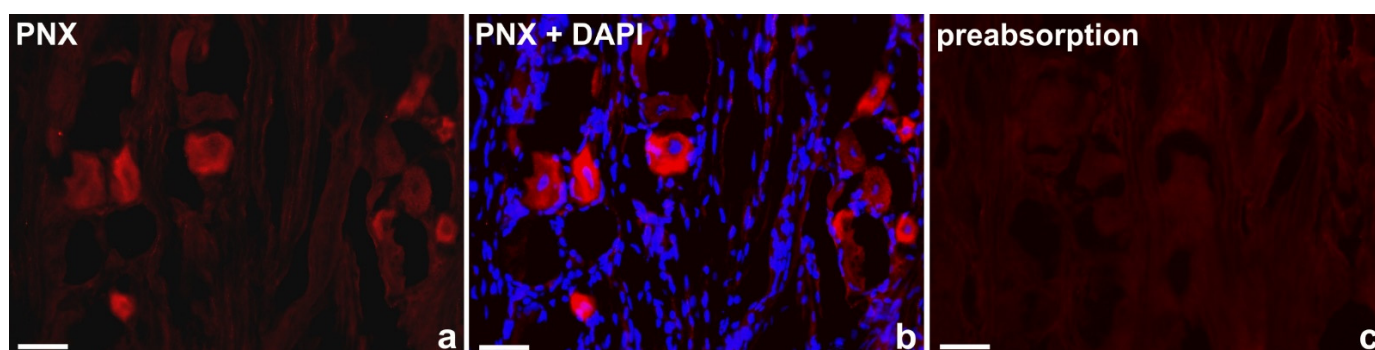


Figure 9. Representative examples of the immunofluorescence staining specificity control procedures used in the study: (a) “classical” staining with anti-PNX antibody, visualized by CY3, (b) anti-PNX antibody + 4',6-diamidino-2-phenylindole (DAPI) as a counterstain, (c) antiserum anti-PNX antibody preabsorbed with PNX amide. Scale bar: 50 μ m.

5. Conclusions

In summary, our research is the second work to show the location of PNX in DRGs, and the first performed in a large mammal (pig). Moreover, we have revealed the coexistence pattern(s) of PNX with a plethora of other neurotransmitters in the examined nerve cells, suggesting the existence of multiple transmitters using DRG cells (i.e., PNX/CGRP/SP/NOS/CART), that may, most probably, be involved in the control of blood vessel tone, maintenance/regulation of neurogenic inflammation process, as well as in the conveyance of itching sensations. These data may be helpful in better understanding the functional role of PNX in transmitting various types of sensory information and its possible impact on the functioning of many organs in the body. Additionally, the presented data indicate that PNX-IR appears in a heterogeneous group of sensory ganglion cells, from small to large, suggesting that this peptide can be subordinated to different sensory modalities.

Supplementary Materials: The supporting information can be downloaded at: <https://www.mdpi.com/article/10.3390/ijms242316647/s1>.

Author Contributions: Conceptualization, A.B. and M.K.M.; methodology, A.B.; validation, A.B. and E.L.-B.; surgical procedures, A.B., E.L. and M.K.M.; formal analysis, U.M. and A.B.; investigation, U.M. and P.J.; resources, U.M. and A.B.; writing—original draft preparation, U.M. and A.B.; writing—review and editing, A.B., E.L. and M.K.M.; visualization, U.M., E.L. and E.L.-B.; supervision, A.B.; project administration, U.M. and A.B.; funding acquisition, A.B. All authors have read and agreed to the published version of the manuscript.

Funding: Agnieszka Bossowska was the recipient of the Statutory Fund of the School of Medicine, Collegium Medicum (61.610.008-110), University of Warmia and Mazury in Olsztyn.

Institutional Review Board Statement: The study was conducted in accordance with the Declaration of Helsinki and approved by the Ethics Committee for Animal Experimentation in Olsztyn, Poland (affiliated with the National Ethics Committee for Animal Experimentation, Polish Ministry of Science and Higher Education; decision No. 40/2020 from 22 July 2020).

Informed Consent Statement: Not applicable.

Data Availability Statement: The data that support the findings of this study are available from the corresponding author upon reasonable request.

Conflicts of Interest: The authors declare no conflict of interest. The funders had no role in the design of the study; in the collection, analyses or interpretation of data; in the writing of the manuscript; or in the decision to publish the results.

References

1. Yosten, G.L.C.; Lyu, R.M.; Hsueh, A.J.W.; Avsian-Kretschmer, O.; Chang, J.K.; Tullock, C.W.; Dun, S.L.; Dun, N.; Samson, W.K. A Novel Reproductive Peptide, Phoenixin. *J. Neuroendocr.* **2013**, *25*, 206–215. [[CrossRef](#)] [[PubMed](#)]
2. Treen, A.K.; Luo, V.; Belsham, D.D. Phoenixin Activates Immortalized GnRH and Kisspeptin Neurons through the Novel Receptor GPR173. *Mol. Endocrinol.* **2016**, *30*, 872–888. [[CrossRef](#)] [[PubMed](#)]
3. McIlwraith, E.K.; Zhang, N.; Belsham, D.D. The Regulation of Phoenixin: A Fascinating Multidimensional Peptide. *J. Endocr. Soc.* **2022**, *6*, bvab192. [[CrossRef](#)] [[PubMed](#)]
4. Liang, H.; Zhao, Q.; Lv, S.; Ji, X. Regulation and Physiological Functions of Phoenixin. *Front. Mol. Biosci.* **2022**, *9*, 956500. [[CrossRef](#)] [[PubMed](#)]
5. Lyu, R.M.; Huang, X.F.; Zhang, Y.; Dun, S.L.; Luo, J.J.; Chang, J.K.; Dun, N.J. Phoenixin: A Novel Peptide in Rodent Sensory Ganglia. *Neuroscience* **2013**, *250*, 622–631. [[CrossRef](#)]
6. Lepiarczyk, E.; Bossowska, A.; Majewska, M.; Skowrońska, A.; Kaleczyc, J.; Majewski, M. Distribution and Chemical Coding of Phoenixin-Immunoreactive Nerve Structures in the Spinal Cord of the Pig. *Ann. Anat.* **2020**, *232*, 151559. [[CrossRef](#)]
7. Dalmoose, A.L.; Hvistendahl, J.J.; Olsen, L.H.; Eskild-Jensen, A.; Djurhuus, J.C.; Swindle, M.M. Surgically Induced Urologic Models in Swine. *J. Investig. Surg.* **2000**, *13*, 133–145. [[CrossRef](#)]
8. Kuzmuk, K.N.; Schook, L.B. Pigs as a Model for Biomedical Sciences. In *The Genetics of the Pig*, 2nd ed.; CABI: Wallingford, UK, 2011; pp. 426–444. [[CrossRef](#)]
9. Swindle, M.M.; Makin, A.; Herron, A.J.; Clubb, F.J.; Frazier, K.S. Swine as Models in Biomedical Research and Toxicology Testing. *Vet. Pathol.* **2012**, *49*, 344–356. [[CrossRef](#)]
10. Gromadziński, L.; Skowrońska, A.; Holak, P.; Smoliński, M.; Lepiarczyk, E.; Żurada, A.; Majewski, M.K.; Skowroński, M.T.; Majewska, M. A New Experimental Porcine Model of Venous Thromboembolism. *J. Clin. Med.* **2021**, *10*, 1862. [[CrossRef](#)]
11. Prinz, P.; Scharner, S.; Friedrich, T.; Schalla, M.; Goebel-Stengel, M.; Rose, M.; Stengel, A. Central and Peripheral Expression Sites of Phoenixin-14 Immunoreactivity in Rats. *Biochem. Biophys. Res. Commun.* **2017**, *493*, 195–201. [[CrossRef](#)]
12. D’Mello, R.; Dickenson, A.H. Spinal Cord Mechanisms of Pain. *Br. J. Anaesth.* **2008**, *101*, 8–16. [[CrossRef](#)]
13. Cowan, A.; Lyu, R.M.; Chen, Y.H.; Dun, S.L.; Chang, J.K.; Dun, N.J. Phoenixin: A Candidate Pruritogen in the Mouse. *Neuroscience* **2015**, *310*, 541–548. [[CrossRef](#)]
14. Bossowska, A.; Crayton, R.; Radziszewski, P.; Kmiec, Z.; Majewski, M. Distribution and Neurochemical Characterization of Sensory Dorsal Root Ganglia Neurons Supplying Porcine Urinary Bladder. *J. Physiol. Pharmacol.* **2009**, *60* (Suppl. S4), 77–81.
15. Cheng, X.; Xiao, F.; Xie, R.; Hu, H.; Wan, Y. Alternate Thermal Stimulation Ameliorates Thermal Sensitivity and Modulates Calbindin-D 28K Expression in Lamina I and II and Dorsal Root Ganglia in a Mouse Spinal Cord Contusion Injury Model. *FASEB J.* **2021**, *35*, e21173. [[CrossRef](#)]
16. Cervero, F.; Iggo, A. The substantia gelatinosa of the spinal cord: A critical review. *Brain* **1980**, *103*, 717–772. [[CrossRef](#)] [[PubMed](#)]
17. Gibson, S.J.; Polak, J.M.; Bloom, S.R.; Sabate, P.M.; Mulderry, P.M.; Ghatei, M.A.; McGregor, G.P.; Morrison, J.F.B.; Kelly, J.S.; Evans, R.M.; et al. Calcitonin gene-related peptide immunoreactivity in the spinal cord of man and of eight other species. *J. Neurosci.* **1984**, *4*, 3101–3111. [[CrossRef](#)]
18. Nordlind, K.; Eriksson, L.; Seiger, Å.; Bakhtiet, M. Expression of Interleukin-6 in Human Dorsal Root Ganglion Cells. *Neurosci. Lett.* **2000**, *280*, 139–142. [[CrossRef](#)] [[PubMed](#)]
19. Nakamura, K.; Ajijola, O.A.; Aliotta, E.; Armour, J.A.; Ardell, J.L.; Shivkumar, K. Pathological effects of chronic myocardial infarction on peripheral neurons mediating cardiac neurotransmission. *Auton. Neurosci.* **2016**, *197*, 34–40. [[CrossRef](#)] [[PubMed](#)]
20. Javed, H.; Rehmathulla, S.; Tariq, S.; Ali, M.A.; Emerald, B.S.; Shehab, S. Co-Localization of Nociceptive Markers in the Lumbar Dorsal Root Ganglion and Spinal Cord of Dromedary Camel. *J. Comp. Neurol.* **2021**, *529*, 3710–3725. [[CrossRef](#)]
21. Giaid, A.; Gibson, S.J.; Ibrahim, N.B.N.; Legon, S.; Bloom, S.R.; Yanagisawa, M.; Masaki, T.; Varndell, I.M.; Polak, J.M. Endothelin 1, an Endothelium-Derived Peptide, Is Expressed in Neurons of the Human Spinal Cord and Dorsal Root Ganglia. *Proc. Natl. Acad. Sci. USA* **1989**, *86*, 7634–7638. [[CrossRef](#)] [[PubMed](#)]

22. Landry, M.; Åman, K.; Dostrovsky, J.; Lozano, A.M.; Carlstedt, T.; Spenger, C.; Josephson, A.; Wiesenfeld-Hallin, Z.; Hökfelt, T. Galanin Expression in Adult Human Dorsal Root Ganglion Neurons: Initial Observations. *Neuroscience* **2003**, *117*, 795–809. [[CrossRef](#)]
23. Merighi, A.; Kar, S.; Gibson, S.J.; Ghidella, S.; Gobetto, A.; Peirone, S.M.; Polak, J.M. The Immunocytochemical Distribution of Seven Peptides in the Spinal Cord and Dorsal Root Ganglia of Horse and Pig. *Anat. Embryol.* **1990**, *181*, 271–280. [[CrossRef](#)] [[PubMed](#)]
24. Iyengar, S.; Johnson, K.W.; Ossipov, M.H.; Aurora, S.K. CGRP and the Trigeminal System in Migraine. *Headache* **2019**, *59*, 659–681. [[CrossRef](#)]
25. Dodds, K.N.; Kyloh, M.A.; Travis, L.; Cox, M.; Hibberd, T.J.; Spencer, N.J. Anatomical Distribution of CGRP-Containing Lumbosacral Spinal Afferent Neurons in the Mouse Uterine Horn. *Front. Neurosci.* **2022**, *16*, 1012329. [[CrossRef](#)]
26. Brain, S.D.; Tippins, J.R.; Morris, H.R.; MacIntyre, I.; Williams, T.J. Potent Vasodilator Activity of Calcitonin Gene-Related Peptide in Human Skin. *J. Investig. Derm.* **1986**, *87*, 533–536. [[CrossRef](#)]
27. Bunker, C.B.; Reavley, C.; Dowd, P.M.; O’Shaughnessy, D.J. Calcitonin Gene-Related Peptide in Treatment of Severe Peripheral Vascular Insufficiency in Raynaud’s Phenomenon. *Lancet* **1993**, *342*, 80–83. [[CrossRef](#)]
28. Mitsikostas, D.D.; Reuter, U. Calcitonin Gene-Related Peptide Monoclonal Antibodies for Migraine Prevention: Comparisons across Randomized Controlled Studies. *Curr. Opin. Neurol.* **2017**, *30*, 272–280. [[CrossRef](#)]
29. Garry, M.G.; Hargreaves, K.M. Enhanced Release of Immunoreactive CGRP and Substance P from Spinal Dorsal Horn Slices Occurs during Carrageenan Inflammation. *Brain Res.* **1992**, *582*, 139–142. [[CrossRef](#)]
30. Kawasaki, H.; Takasaki, K.; Saito, A.; Goto, K. Calcitonin Gene-Related Peptide Acts as a Novel Vasodilator Neurotransmitter in Mesenteric Resistance Vessels of the Rat. *Nature* **1988**, *335*, 164–167. [[CrossRef](#)] [[PubMed](#)]
31. Cao, T.; Pintér, E.; Al-Rashed, S.; Gerard, N.; Hoult, J.R.; Brain, S.D. Neurokinin-1 Receptor Agonists Are Involved in Mediating Neutrophil Accumulation in the Inflamed, but Not Normal, Cutaneous Microvasculature: An in Vivo Study Using Neurokinin-1 Receptor Knockout Mice. *J. Immunol.* **2000**, *164*, 5424–5429. [[CrossRef](#)] [[PubMed](#)]
32. Biella, G.; Panara, C.; Pecile, A.; Sotgiu, M.L. Facilitatory Role of Calcitonin Gene-Related Peptide (CGRP) on Excitation Induced by Substance P (SP) and Noxious Stimuli in Rat Spinal Dorsal Horn Neurons. An Iontophoretic Study in Vivo. *Brain Res.* **1991**, *559*, 352–356. [[CrossRef](#)]
33. Le Grevés, P.; Nyberg, F.; Hökfelt, T.; Terenius, L. Calcitonin Gene-Related Peptide Is Metabolized by an Endopeptidase Hydrolyzing Substance P. *Regul. Pept.* **1989**, *25*, 277–286. [[CrossRef](#)] [[PubMed](#)]
34. Le Greves, P.; Nyberg, F.; Terenius, L.; Hökfelt, T. Calcitonin Gene-Related Peptide Is a Potent Inhibitor of Substance P Degradation. *Eur. J. Pharmacol.* **1985**, *115*, 309–311. [[CrossRef](#)] [[PubMed](#)]
35. Oku, R.; Satoh, M.; Fujii, N.; Otaka, A.; Yajima, H.; Takagi, H. Calcitonin Gene-Related Peptide Promotes Mechanical Nociception by Potentiating Release of Substance P from the Spinal Dorsal Horn in Rats. *Brain Res.* **1987**, *403*, 350–354. [[CrossRef](#)] [[PubMed](#)]
36. Kangrga, I.; Larew, J.S.A.; Randic, M. The Effects of Substance P and Calcitonin Gene-Related Peptide on the Efflux of Endogenous Glutamate and Aspartate from the Rat Spinal Dorsal Horn in Vitro. *Neurosci. Lett.* **1990**, *108*, 155–160. [[CrossRef](#)]
37. Cooper, D.; Laidig, W.D.; Sappington, A.; MacGregor, G. A Pharmacological Review of Calcitonin Gene-Related Peptide Biologics and Future Use for Chronic Pain. *Cureus* **2023**, *15*, e35109. [[CrossRef](#)]
38. Nicoll, R.A.; Schenker, C.; Leeman, S.E. Substance P as a Transmitter Candidate. *Annu. Rev. Neurosci.* **1980**, *3*, 227–268. [[CrossRef](#)]
39. Lawson, S.N.; Crepps, B.A.; Perl, E.R. Relationship of Substance P to Afferent Characteristics of Dorsal Root Ganglion Neurons in Guinea-Pig. *J. Physiol.* **1997**, *505*, 177–191. [[CrossRef](#)]
40. Janikiewicz, P.; Wasilewska, B.; Mazur, U.; Franke-Radowiecka, A.; Majewski, M.; Bossowska, A. The Influence of an Adrenergic Antagonist Guanethidine (GUA) on the Distribution Pattern and Chemical Coding of Dorsal Root Ganglia (DRG) Neurons Supplying the Porcine Urinary Bladder. *Int. J. Mol. Sci.* **2021**, *22*, 13399. [[CrossRef](#)]
41. Han, D.S.; Lee, C.H.; Shieh, Y.D.; Chang, C.T.; Li, M.H.; Chu, Y.C.; Wang, J.L.; Chang, K.V.; Lin, S.H.; Chen, C.C. A Role for Substance P and Acid-Sensing Ion Channel 1a in Prolotherapy with Dextrose-Mediated Analgesia in a Mouse Model of Chronic Muscle Pain. *Pain* **2022**, *163*, E622–E633. [[CrossRef](#)]
42. Kozłowska, A.; Mikołajczyk, A.; Adamiak, Z.; Majewski, M. Distribution and Chemical Coding of Sensory Neurons Innervating the Skin of the Porcine Hindlimb. *Neuropeptides* **2017**, *61*, 1–14. [[CrossRef](#)]
43. McCarthy, P.W.; Lawson, S.N. Cell Type and Conduction Velocity of Rat Primary Sensory Neurons with Substance P-like Immunoreactivity. *Neuroscience* **1989**, *28*, 745–753. [[CrossRef](#)] [[PubMed](#)]
44. Simões, A.L.B.; Silva, G.A.R.; Giorgetto, C.; de Cassia do Carmo-Campos, E.; Dias, F.J.; Fazan, V.P.S. Substance P in Dorsal Root Ganglion Neurons in Young and Adult Rats, after Nociceptive Stimulation during the Neonatal Period. *Anat. Rec.* **2018**, *301*, 849–861. [[CrossRef](#)] [[PubMed](#)]
45. Kourosh-Armani, M.; Hosseini, N.; Mohsenzadegan, M.; Komaki, A.; Joghataei, M.T. Neurophysiological Implications of Neuronal Nitric Oxide Synthase. *Rev. Neurosci.* **2020**, *31*, 617–636. [[CrossRef](#)]
46. Zhou, L.; Zhu, D.Y. Neuronal Nitric Oxide Synthase: Structure, Subcellular Localization, Regulation, and Clinical Implications. *Nitric Oxide* **2009**, *20*, 223–230. [[CrossRef](#)] [[PubMed](#)]
47. Thippeswamy, T.; Morris, R. The Roles of Nitric Oxide in Dorsal Root Ganglion Neurons. *Ann. N. Y. Acad. Sci.* **2002**, *962*, 103–110. [[CrossRef](#)] [[PubMed](#)]
48. Zheng, Q.; Dong, X.; Green, D.P.; Dong, X. Peripheral Mechanisms of Chronic Pain. *Med. Rev.* **2022**, *2*, 251–270. [[CrossRef](#)]

49. Rocha, P.A.; Ferreira, A.F.B.; Da Silva, J.T.; Alves, A.S.; Martins, D.O.; Britto, L.R.G.; Chacur, M. Effects of Selective Inhibition of NNOS and iNOS on Neuropathic Pain in Rats. *Mol. Cell. Neurosci.* **2020**, *105*, 103497. [[CrossRef](#)]
50. Solanki, K.; Rajpoot, S.; Bezsonov, E.E.; Orekhov, A.N.; Saluja, R.; Wary, A.; Axen, C.; Wary, K.; Baig, M.S. The Expanding Roles of Neuronal Nitric Oxide Synthase (NOS1). *PeerJ* **2022**, *10*, e13651. [[CrossRef](#)]
51. Terenghi, G.; Riveros-Moreno, V.; Hudson, L.D.; Ibrahim, N.B.N.; Polak, J.M. Immunohistochemistry of Nitric Oxide Synthase Demonstrates Immunoreactive Neurons in Spinal Cord and Dorsal Root Ganglia of Man and Rat. *J. Neurol. Sci.* **1993**, *118*, 34–37. [[CrossRef](#)]
52. Tan, L.L.; Bornstein, J.C.; Anderson, C.R. Distinct Chemical Classes of Medium-Sized Transient Receptor Potential Channel Vanilloid 1-Immunoreactive Dorsal Root Ganglion Neurons Innervate the Adult Mouse Jejunum and Colon. *Neuroscience* **2008**, *156*, 334–343. [[CrossRef](#)] [[PubMed](#)]
53. Russo, D.; Clavenzani, P.; Mazzoni, M.; Chiocchetti, R.; Di Guardo, G.; Lalatta-Costerbosa, G. Immunohistochemical Characterization of TH13-L2 Spinal Ganglia Neurons in Sheep (*Ovis aries*). *Microsc. Res. Tech.* **2010**, *73*, 128–139. [[CrossRef](#)] [[PubMed](#)]
54. Wiesenfeld-Hallin, Z.; Xu, X.J. Galanin in Somatosensory Function. *Ann. N. Y. Acad. Sci.* **1998**, *863*, 383–389. [[CrossRef](#)] [[PubMed](#)]
55. Hökfelt, T.; Wiesenfeld-Hallin, Z.; Villar, M.; Melander, T. Increase of Galanin-like Immunoreactivity in Rat Dorsal Root Ganglion Cells after Peripheral Axotomy. *Neurosci. Lett.* **1987**, *83*, 217–220. [[CrossRef](#)]
56. Hao, J.-X.; Shi, T.-J.; Xu, I.S.; Kaupilla, T.; Xu, X.-J.; Hökfelt, T.; Bartfai, T.; Wiesenfeld-Hallin, Z. Intrathecal Galanin Alleviates Allodynia-like Behaviour in Rats after Partial Peripheral Nerve Injury. *Eur. J. Neurosci.* **1999**, *11*, 427–432. [[CrossRef](#)]
57. Metcalf, C.S.; Klein, B.D.; McDougale, D.R.; Zhang, L.; Smith, M.D.; Bulaj, G.; White, H.S. Analgesic Properties of a Peripherally Acting and GalR2 Receptor-Preferring Galanin Analog in Inflammatory, Neuropathic, and Acute Pain Models. *J. Pharmacol. Exp. Ther.* **2015**, *352*, 185–193. [[CrossRef](#)]
58. Lang, R.; Gundlach, A.L.; Holmes, F.E.; Hobson, S.A.; Wynick, D.; Hökfelt, T.; Kofler, B. Physiology, Signaling, and Pharmacology of Galanin Peptides and Receptors: Three Decades of Emerging Diversity. *Pharmacol. Rev.* **2015**, *67*, 118–175. [[CrossRef](#)]
59. Moller, K.; Zhang, Y.Z.; Håkanson, R.; Luts, A.; Sjölund, B.; Uddman, R.; Sundler, F. Pituitary Adenylate Cyclase Activating Peptide Is a Sensory Neuropeptide: Immunocytochemical and Immunochemical Evidence. *Neuroscience* **1993**, *57*, 725–732. [[CrossRef](#)]
60. Zhang, Q.; Shi, T.J.; Ji, R.R.; Zhang, Y.; Sundler, F.; Hannibal, J.; Fahrenkrug, J.; Hökfelt, T. Expression of Pituitary Adenylate Cyclase-Activating Polypeptide in Dorsal Root Ganglia Following Axotomy: Time Course and Coexistence. *Brain Res.* **1995**, *705*, 149–158. [[CrossRef](#)]
61. Mulder, H.; Uddman, R.; Moller, K.; Zhang, Y.Z.; Ekblad, E.; Alumets, J.; Sundler, F. Pituitary Adenylate Cyclase Activating Polypeptide Expression in Sensory Neurons. *Neuroscience* **1994**, *63*, 307–312. [[CrossRef](#)]
62. Corness, J.; Shi, T.J.; Xu, Z.Q.; Brulet, P.; Hökfelt, T. Influence of Leukemia Inhibitory Factor on Galanin/GMAP and Neuropeptide Y Expression in Mouse Primary Sensory Neurons after Axotomy. *Exp. Brain Res.* **1996**, *112*, 79–88. [[CrossRef](#)] [[PubMed](#)]
63. Lioudyno, M.; Skoglösa, Y.; Takei, N.; Lindholm, D. Rapid Communication Pituitary Adenylate Cyclase-Activating Polypeptide (PACAP) Protects Dorsal Root Ganglion Neurons From Death and Induces Calcitonin Gene-Related Peptide (CGRP) Immunoreactivity In Vitro. *J. Neurosci. Res.* **1998**, *51*, 243–256. [[CrossRef](#)]
64. Xu, X.; Yang, X.; Zhang, P.; Chen, X.; Liu, H.; Li, Z. Effects of Exogenous Galanin on Neuropathic Pain State and Change of Galanin and Its Receptors in DRG and SDH after Sciatic Nerve-Pinch Injury in Rat. *PLoS ONE* **2012**, *7*, e37621. [[CrossRef](#)]
65. Zacharko-Siembida, A.; Kulik, P.; Szalak, R.; Lalak, R.; Arciszewski, M.B. Co-Expression Patterns of Cocaine- and Amphetamine-Regulated Transcript (CART) with Neuropeptides in Dorsal Root Ganglia of the Pig. *Acta Histochem.* **2014**, *116*, 390–398. [[CrossRef](#)]
66. Kozsurek, M.; Lukácsi, E.; Fekete, C.; Wittmann, G.; Réthelyi, M.; Puskár, Z. Cocaine- and Amphetamine-Regulated Transcript Peptide (CART) Is Present in Peptidergic C Primary Afferents and Axons of Excitatory Interneurons with a Possible Role in Nociception in the Superficial Laminae of the Rat Spinal Cord. *Eur. J. Neurosci.* **2007**, *26*, 1624–1631. [[CrossRef](#)]
67. Hökfelt, T.; Elde, R.; Johansson, O.; Luft, R.; Nilsson, G.; Arimura, A. Immunohistochemical Evidence for Separate Populations of Somatostatin-Containing and Substance P-Containing Primary Afferent Neurons in the Rat. *Neuroscience* **1976**, *1*, 131–136, IN19–IN24. [[CrossRef](#)] [[PubMed](#)]
68. Kardon, A.P.; Polgár, E.; Hachisuka, J.; Snyder, L.M.; Cameron, D.; Savage, S.; Cai, X.; Karnup, S.; Fan, C.R.; Hemenway, G.M.; et al. Dynorphin Acts as a Neuromodulator to Inhibit Itch in the Dorsal Horn of the Spinal Cord. *Neuron* **2014**, *82*, 573–586. [[CrossRef](#)]
69. Stantcheva, K.K.; Iovino, L.; Dhandapani, R.; Martinez, C.; Castaldi, L.; Nocchi, L.; Perlas, E.; Portulano, C.; Pesaresi, M.; Shirlekar, K.S.; et al. A Subpopulation of Itch-Sensing Neurons Marked by Ret and Somatostatin Expression. *EMBO Rep.* **2016**, *17*, 585–600. [[CrossRef](#)]
70. Friedrich, T.; Stengel, A. Current State of Phoenixin—the Implications of the Pleiotropic Peptide in Stress and Its Potential as a Therapeutic Target. *Front. Pharmacol.* **2023**, *14*, 1076800. [[CrossRef](#)]
71. Antal, M.; Polgár, E.; Chalmers, J.; Minson, J.B.; Llewellyn-Smith, I.; Heizmann, C.W.; Somogyi, P. Different Populations of Parvalbumin- and Calbindin-D28k-Immunoreactive Neurons Contain GABA and Accumulate 3H-D-Aspartate in the Dorsal Horn of the Rat Spinal Cord. *J. Comp. Neurol.* **1991**, *314*, 114–124. [[CrossRef](#)] [[PubMed](#)]

72. Egea, J.; Malmierca, E.; Rosa, A.O.; Del Barrio, L.; Negrodo, P.; Nuñez, A.; López, M.G. Participation of Calbindin-D28K in Nociception: Results from Calbindin-D28K Knockout Mice. *Pflug. Arch.* **2012**, *463*, 449–458. [[CrossRef](#)]
73. Ren, K.; Ruda, M.A.; Jacobowitz, D.M. Immunohistochemical Localization of Calretinin in the Dorsal Root Ganglion and Spinal Cord of the Rat. *Brain Res. Bull.* **1993**, *31*, 13–22. [[CrossRef](#)] [[PubMed](#)]
74. Stebbing, M.J.; Balasubramanyan, S.; Smith, P.A. Calbindin-D-28K like Immunoreactivity in Superficial Dorsal Horn Neurons and Effects of Sciatic Chronic Constriction Injury. *Neuroscience* **2016**, *324*, 330–343. [[CrossRef](#)] [[PubMed](#)]
75. Ichikawa, H.; Jacobowitz, D.M.; Sugimoto, T. Calretinin-Immunoreactive Neurons in the Trigeminal and Dorsal Root Ganglia of the Rat. *Brain Res.* **1993**, *617*, 96–102. [[CrossRef](#)] [[PubMed](#)]

Disclaimer/Publisher’s Note: The statements, opinions and data contained in all publications are solely those of the individual author(s) and contributor(s) and not of MDPI and/or the editor(s). MDPI and/or the editor(s) disclaim responsibility for any injury to people or property resulting from any ideas, methods, instructions or products referred to in the content.